CHAPTER 9: EVALUATION OF MINERALS, FLUIDS AND IN-SITU ENVIRONMENTS.

SECTION 9A: OIL & GAS

9A.1. GENERAL INTRODUCTION

9A.2. EVALUATIONS FOR OIL AND GAS
    9A.2.1. Reservoir delineation
    9A.2.2. Natural gamma radiation (GR)
    9A.2.3. Spontaneous potential (SP)
    9A.2.4. Micro-resistivity tools (MLL)
    9A.2.5. Net over gross (n/g)
    9A.2.6. Porosity determination
        9A.2.6.1. Density log
        9A.2.6.2. Sonic log
        9A.2.6.3. Neutron log
    9A.2.7. Gas effect
        9A.2.7.1. Neutron log
        9A.2.7.2. Density log
    9A.2.8. Lithology
        9A.2.8.1. Single log
        9A.2.8.2. Two logs / Porosity cross-plots
        9A.2.8.3. Shaly snds
    9A.2.9. Saturation determination from logs
    9A.2.10. Fuid contacts
        9A.2.10.1. Wireline Formation Testing
        9A.2.10.2. Log saturation profiles and capillary pressure
                curves
        9A.2.11. Hydrocarbon reserves volume estimation

SECTION 9B: COAL & WATER

9B.1. GENERAL INTRODUCTION

9B.2. EVALUATION OF COAL SEAMS
9B.2.1. Introduction & history
9B.2.2. Coal quality
9B.2.3. Ash content
9B.2.4. Moisture content
9B.2.5. Floats/sinks, calorific value, volatiles, sulphur
9B.2.6. Coalbed methane
9B.2.7. Lignite (brown) coal

9B.3. EVALUATION OF GROUNDWATER
9B.3.1. Introduction and history
9B.3.2. Logging tools in open water wells: methodology
9B.3.3. Parameters regarding the condition of water
9B.3.4. The interpretation of log information
    9B.3.4.1. General aspects
    9B.3.4.2. Aquifer position & net over gross
    9B.3.4.3. Lithology
    9B.3.4.4. Water salinity & hardness of aquifers
    9B.3.4.5. Porosity of aquifers
    9B.3.4.6. Permeability & grain—size distribution

9B.3.5. Cased hole log interpretation
    9B.3.5.1. The Spinner
    9B.3.5.2. Conductivity & thermal flow meters
    9B.3.5.3. Video & flow-vision (video flow meter logs)
    9B.3.5.4. Borehole televiewer
    9B.3.5.5. Permanently installed electrode arrays

9B.1 GENERAL INTRODUCTION ON THE EVALUATION OF OIL AND GAS

In this chapter the evaluation of wireline logs for oil and gas reservoirs, coal, groundwater and ores, will be discussed. As mentioned in the general introduction impressive progress was made during the last decade in the interpretation of geophysical measurements, which were made at the surface. Direct coal, ore, hydrocarbon or groundwater indicators can frequently be derived from surface seismic, provided accurate well data over the area of interest is available for calibration. For exploration and appraisal activities direct physical contact with the prospective layers is even now required to resolve the question whether profitable occurrences are present. In Chapter 3, committed to various methods of formation evaluation, the analysis of drill cuttings and cores was discussed. These methods are common for the four petrophysical application areas covered in these lectures:

- hydrocarbons,
- coal,
- groundwater, and
- minerals and/or mechanical properties.

This section 9A will concentrate on the analysis of wireline logs to determine the hydrocarbon reservoir parameters as listed in table 9A.1.

9B.2 EVALUATIONS FOR OIL AND GAS

Wells have to be drilled to penetrate (profitable) oil and gas layers, to get direct physical evidence from drill cuttings, hydrocarbon in the mud, core samples, and production tests, or indirectly from wireline logging measurements. Table 9A.1 lists the reservoir parameters that have to be deduced from the data based on cores, logs, cutting descriptions, and production & wireline tests.

9B.2.1 RESERVOIR DELINEATION

For a sedimentary layer to be a potential reservoir it should have both porosity (storage capacity) and permeability (fluid flow capacity). When core samples are not (yet) available only a combination of several different wireline-logging measurements can give a good indication whether both conditions are fulfilled. For conventional evaluations the following tools are used to distinguish reservoirs:
- the natural gamma radiation tool (GR),
- the spontaneous potential tool (SP), and
- a combination of micro-resistivity readings to prove invasion of mud-filtrate.

The principles of these tools were discussed in Chapters 5, 6, 7 and 8.

LOCATE:	Reservoir non-reservoir
DETECT:	fluid content water/oil/gas
EVALUATE:	lithology porosity permeability capillary properties mechanical strength salinity of the water original hydrocarbon saturation movable hydrocarbons residual hydrocarbons % oil / gas / water gross / net thickness reservoir pressure

Table 9A. 1: Objectives of a petrophysical interpretation

9B.2.2 NATURAL GAMMA RADIATION (GR)

Shale, clays, and silts usually have no reservoir potential due to their very low permeability (μD range). Nature has been kind because these sediments, as a rule, accumulate much more natural radioactive minerals (uranium U, thorium Th, and potassium K isotopes) than clean porous sand, limestone, and dolomite layers, in which the majority of producable hydrocarbons are stored.

Separating layers with a high natural radiation level from layers with a low level is usually the first step in log analysis. In this way shale layers and potential reservoir layers are recognised.

An example of this division is shown in Figure 6.6. for a sand/shale sequence. The separation between the GR log deflection in a clean sand and in a 100% shale interval can be used to estimate the shale content in the shaly sand layers as discussed in the chapters 6 and 8.

Sometimes the presence of mica, which has a high natural gamma-radiation, can mask the presence of reservoir sands with a high oil production potential. The use of spectral gamma-ray logs that can separate the contributions of U, Th, and K, in combination with the photoelectric absorption coefficient P_e, is applied to recognise the occurrence of these minerals. This method will be discussed in the second part (third year petroleum engineering & geophysics) of this lecture series.

9B.2.3 SPONTANEOUS POTENTIAL (SP)

The physical phenomena that underlie the functioning of this tool were discussed in Chapter 5. The difference of salinity between the water in the pores of the reservoir and the salinity of the mud on the one hand and the membrane potential between shales and the porous reservoir on the other hand, produce a combined electrical potential difference in the mud that can be measured with an SP tool. The potential only occurs when ions can move from the mud into the pores, which implies that porosity and a minimum permeability must exist before the spontaneous potential can be detected.

Various examples of the detection of permeable layers and related sedimentary environments are shown in chapter 5. The SP signal is most prominent for fresh water based mud and on-shore wells when a good return of the current to the surface electrode is ensured. It is not surprising that the better SP logs were recorded in the past when both conditions were fulfilled. The SP is one of the few measurements that did not improve in time and senior petrophysicists (prof. M. Peeters) can become very nostalgic about the good old days in the jungle when SP interpretations and human relations were much easier. I prefer nostalgia on an ore body in Lapland (K-H. Wolf).

9B.2.4 MICRO-RESISTIVITY TOOLS (MLL)

This tool was originally designed to record the resistivity of the invaded zone with two depths of investigation. In its most simple form it had one current and two voltage measuring electrodes with electrodes spacings of approximately 1" as shown in chapter 5. The resistivity measured with the proximate pair of electrodes (micro-normal curve) proved to be much lower than the resistivity measured with the outlying pair (micro-inverse curve) when permeable reservoir sand is present. This came initially as a surprise but could be explained readily by the presence of the high conductive mudcake, which consists often for more than 50% of mud-filtrate. This mudcake affects the shallow measuring pair much more than the deeper measuring pair of electrodes.

Obviously mudcakes can only be deposited when a layer is permeable. The borehole wall then acts as a filter that sieve the solid mud particles from the mud when it invades the reservoir. The separation between the two micro-resistivity curves is therefore an excellent indicator of the presence of a permeable layer. The indication is digital, which means that it only shows the presence or absence of permeability, but does not quantify this parameter. The separation method has the highest vertical resolution of the three reservoir delineation methods discussed in this chapter.

9B.2.5 NET OVER GROSS (N/G)

The reservoir layer thicknesses derived from the SP, GR, MLL or a combination of these tools are added to arrive at the net reservoir thickness "N" contained in the total reservoir depth interval "G", which was surveyed by the logs. The division N/G gives the net over gross ratio.

9B.2.6 POROSITY DETERMINATION

When the porous rock contains only *one fluid*, and *one homogeneous matrix mineral combination*, a "one to one" relation can be established between the porosity and the log readings of the three porosity tools.

9B.2.6.1 DENSITY LOG

For a clean formation of matrix density ρ_{ma} containing a fluid with density ρ_{fl}, the bulk density as measured by the log ρ_b can be expressed as a linear relationship between matrix and fluid points.

$$\rho_b = (1 - \varphi).\rho_{ma} + \varphi.\rho_{fl} \qquad \text{(eq. 9A.1)}$$

Rearranged to:

$$\varphi = \frac{\rho_{ma} - \rho_b}{\rho_{ma} - \rho_{fl}} \qquad \text{(eq. 9A.2)}$$

When the pores contain a mixture of mudfiltrate and hydrocarbons, ρ_{fl} is calculated as follows :

$$\rho_{fl} = S_{xo}.\rho_{mf} + (1 - S_{xo}).\rho_{hc} \qquad \text{(eq. 9A.3)}$$

where;

ρ_b	=	bulk density, g/cc
ϕ	=	porosity, fr.b.v.(fraction of bulk volume)
ρ_{ma}	=	matrix density, g/cc
ρ_{fl}	=	fluid density, g/cc
ρ_{hc}	=	hydrocarbon density, g/cc
ρ_{mf}	=	mudfiltrate density, g/cc
S_{xo}	=	mudfiltrate saturation, fr.p.v. (fraction of pore volume)

The volume fraction of mudfiltrate in the pore space in the flushed zone is usually much larger than that of the hydrocarbons. The hydrocarbon effect is therefore usually small, unless light oil or gas is present. This is further discussed in section 9A.2.7 on the gas effect. In figure 9A.1 the core porosity is plotted versus the bulk density. Extrapolation of the regression line to the intersect with the density axis provides the apparent matrix value, ρ_{ma}.
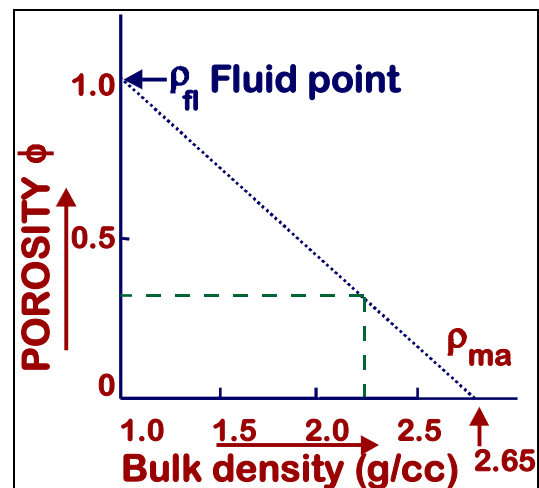

Figure 9A. 1: Core porosity versus bulk density, ρ_b

9B.2.6.2 SONIC LOG

The sonic instruments described in chapter 7 measure the acoustic travel time. For the relation between the travel time of the compressional wave and porosity Wyllie proposed a relation that is equivalent to the relation used for the density log. Transit times increase linearly with porosity according to the Wyllie equation :

$$\Delta T = \varphi.\Delta T_{fl} + (1 - \varphi).\Delta T_{ma} \qquad \text{(eq. 9A.4)}$$

or

$$\varphi = \frac{\Delta T - \Delta T_{ma}}{\Delta T_{fl} - \Delta T_{ma}} \qquad \text{(eq. 9A.5)}$$

where;

ϕ : porosity, fraction of the bulk volume (fr.b.v);

ΔT **:** transit time of the log [or slowness in µs/ft].

    Here the slowness is defined as the reciprocal of the velocity (**1/velocity**);

ΔT_{ma}**:** transit time of the matrix;

ΔT_{fl} **:** transit time of the fluid.

This relationship is displayed in figure 9A.2. Here the porosity versus transit time is exposed for ΔT_{fl}=189 µs/ft. **Note:** The latter value is valid for fresh water or fresh mud filtrate. In the case of unconsolidated (uncompacted) sands the above "Wyllie" equation may give porosity values which are too high. Lack of consolidation is indicated when adjacent shales exhibit ΔT values greater than 100 µs/ft. An empirical correction factor, B_{cp} (refer figure 9A.4), is then applied to the Wyllie equation. B_{cp} is about equal to the reading in shale in µs/ft divided by 100.
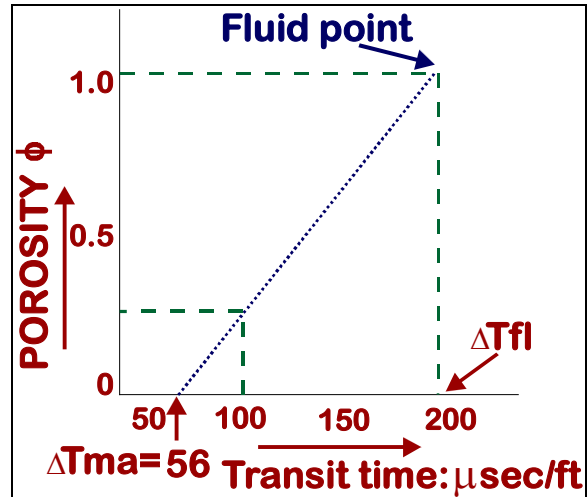

Figure 9A. 2: Graphics display of the Wyllie equation.

The most accurate method to calibrate log porosities obtained with the sonic tool is to compare them with core porosities. Here a good core recovery and a good depth correlation are necessities.

9B.2.6.3 NEUTRON LOGS
The porosity indication provided by the neutron tools is based on the Hydrogen index HI and was discussed in chapter 7. Since the zone of investigation of the neutron tool is often confined to the flushed zone, the porosity derived from the Neutron log (ϕ_n) is related to the true porosity (ϕ) by:

$$\varphi_n = \varphi.(HI_{mf}.S_{xo} + HI_{hc}.(1 - S_{xo})),$$ (eq. 9A.4)

in which HI_{xo} , HI_{mf}, are the hydrogen indices of respectively the residual hydrocarbons in the pores, and the mudfiltrate.

9B.2.7 GAS EFFECT

The presence of gas can be recognised and assessed with the readings of a neutron log and a gamma-gamma or density log

9B.2.7.1 NEUTRON LOG
The gas-effect can be spit into two parts the HYDROGEN effect and the EXCAVATION effect. In these lectures only the hydrogen effect will
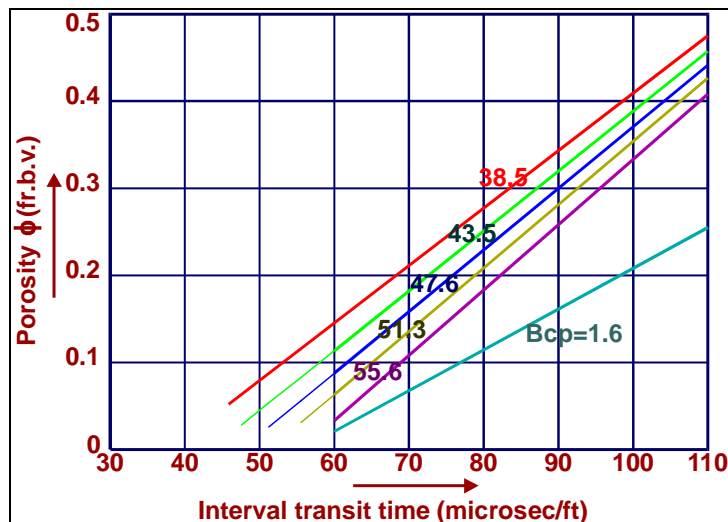

Figure 9A. 3: Graphics presentation of the Wyllie equation

be discussed. The neutron porosity (ϕ_n) is related to the true porosity (ϕ) according to equation 9A.4. The hydrogen index of natural gas (CH_4) for a gas-bearing reservoir at 8000 ft and 200°F is approximately 0.33, and evidently much less than the value "1" which is valid for oil or water. If we assume a formation with a porosity ϕ of 33 % and water saturation S_{xo} in the invaded zone of 70 %, the neutron log reading for this situation is: ϕ_n= 0.33.[1×0.7+0.33×0.3] = 0.26.

Additionally, when the matrix has no effect we would expect the tool to read 0.33 (33 %) if the pores are filled for 100% with water. The depression due to the presence of gas is therefore 7 % b.v.

9B.2.7.2 DENSITY LOG

The resulting *apparent bulk density*, "ρ_a", as seen by the tool, is related to the *electron density* "ρ_e":

$$\rho_a = 1.07.\rho_e - 0.188 \hspace{4cm} \text{(eq. 9A.5)}$$

For liquid filled sandstone, limestone and dolomite the tool reading ρ_a is practically identical to ρ_b. Corrections are required e.g. in anhydrite, sylvite, halite and also in gas bearing formations. For a number of minerals the characteristics were given in tables in chapter 6. The value of ρ_e is the product of 1.238 and the gas density, which is the actual in situ density for CH_4. In practice we assume the gas composition ("natural" gas) to be 90% CH_4 and 10% C_2H_6, and find $\rho_e = 1.238\rho_{gas}$.

Example I:
At a reservoir depth of 8000 ft, with a pressure gradient of 0.44 psi/ft, we find a pressure of 3500 psi. Assuming a temperature of 200°F we find for ρ_{gas} 0.15 g/cc. Hence, ρ_a (gas) = 1.07 x 1.238 x 0.15 - 0.188 = +0.01 g/cc.

Note: *that ρ_a for gas, as seen by the density tool, is much lower than the actual ρ_{gas}*. The effect of gas on the density log, assuming that the investigation depth is shallower than the invasion depth, can be quantified as follows, :
- Mudfiltrate only   : $\rho_b = (1 -\phi)\times\rho_{ma} +\phi\times\rho_{mf}$
- Residual gas   : $\rho_b = (1 -\phi)\times\rho_{ma} +\phi\times S_{xo}\times\rho_{mf} +\phi\times(1-S_{xo})\times\rho_{agas}$

When the density is not corrected for gas the porosity calculated with eq. 14.2 would be too high :

Example II:
ρ_b= 2.11; ρ_{ma} = 2.65; and ρ_{mf} = 1.0 all in g/cc

With no gas present (S_{xo}=1): ϕ=0.33

With S_{xo}=0.70, and ρ_{agas} =+0.01 we find ρ_b = 2.01 g/cc. Using this value to back calculate the porosity with a fluid density of ρ_{fl} of 1 g/cc we find ϕ=0.39
The apparent porosity is therefore 6 % too high.
For the same example the neutron tool reads a 7 % lower porosity i.e. 26 instead of 33 %. **This results in 13 porosity units separation for the porosities derived from density and neutron logs.** Since the gas effects on the density and neutron porosity log readings have opposite direction a large separation is quite common as shown in chapter 7. This negative separation is a very strong gas indicator.

9B.2.8 LITHOLOGY

Lithology determination, i.e. the qualitative mineral content of specific layers already can be done with one single log. For example the SP and GR readings give shale/sand distributions. In addition the shape of the readings give information about the environment of deposition. The accuracy of lithology determination and even quantification of mineral content are possible when two or more (multi) log readings are used.

9B.2.8.1 SINGLE LOG

Many combinations of porosity values and lithology types are possible when only one log is available (figure 9A.4). When it is known from cuttings, cores or other information that only one mineral is present it is no problem to calculate one unique porosity value in a water-bearing reservoir. The

neutron log can be corrected for lithology using a correction chart. For example a neutron log reading of 13 apparent limestone (LST) porosity units converts to 17 % in a sandstone (SST) reservoir and 6% in a dolomite (DOL) reservoir.

It is possible in some reservoirs to obtain the lithology from the acoustic log alone. The ratio of shear transit time (ΔT_s) over compressional transit time (ΔT_c) gives a good indication of lithology provided that shale and gas effects are corrected for. The following values can be useful in the absence of a combination of neutron and density log :

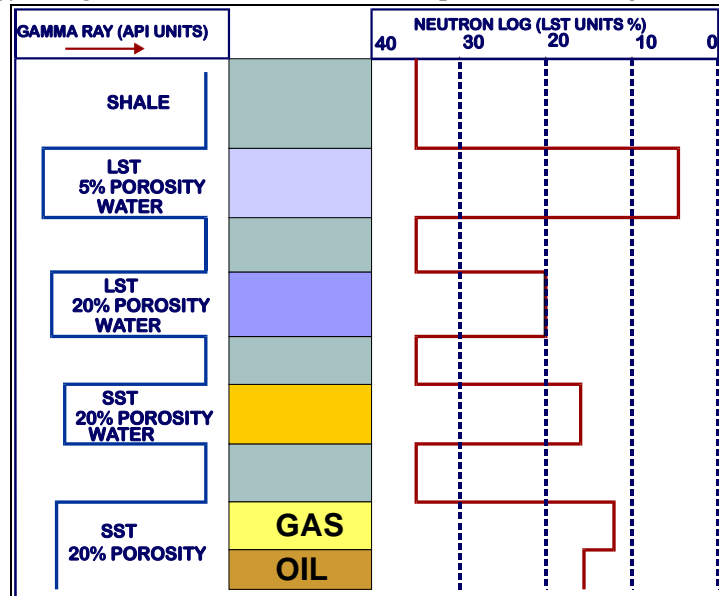| Lithology	$\Delta T_s/\Delta T_c$
Sandstone	1.6
Dolomite	1.8
Limestone	1.9

Figure 9A. 4: Lithology and hydrocarbon effects on the neutron

9B.2.8.2 TWO LOGS / POROSITY CROSS-PLOT

Lithology assessment is often based on a combination of two porosity logs, usually the density and the neutron log. The data from the porosity logs are plotted on a chart the so-called cross-plot. An example for a water bearing formation is shown in figure 9A.5.

If the formation consists of one single lithology, the data points of a water bearing formation fall on the appropriate lithology curve. If the lithology is a mixture of 2 components, e.g. calcite (limestone) and dolomite, the points fall in between 2 lithology curves. This permits identification of the lithologies and determination of their volumetric proportions. Moreover the porosity can be estimated more accurately based on the lithology mix. An example is given by point A in Figure 14.9A. The density log reads ρ_b = 2.48 g/cc and the neutron log ϕ_n = 19 p.u. on the limestone (LST) porosity scale used on the x-axis. This point most likely represents a carbonate interval containing 34% dolomite and 66% limestone. The porosity is found by interpolation to be 16 %. Keeping mind that :

- The position of the top point on the chart could also be interpreted to represent a sandstone-dolomite mixture. Additional information is therefore required to make an unique interpretation.
- The presence of shale and/or hydrocarbons especially gas often requires large corrections to the log readings before the lithological interpretation sketched above can be applied with confidence.

Cross-plots of neutron vs. sonic log readings and density vs. sonic are also infrequently used for simultaneous lithology and porosity determination.
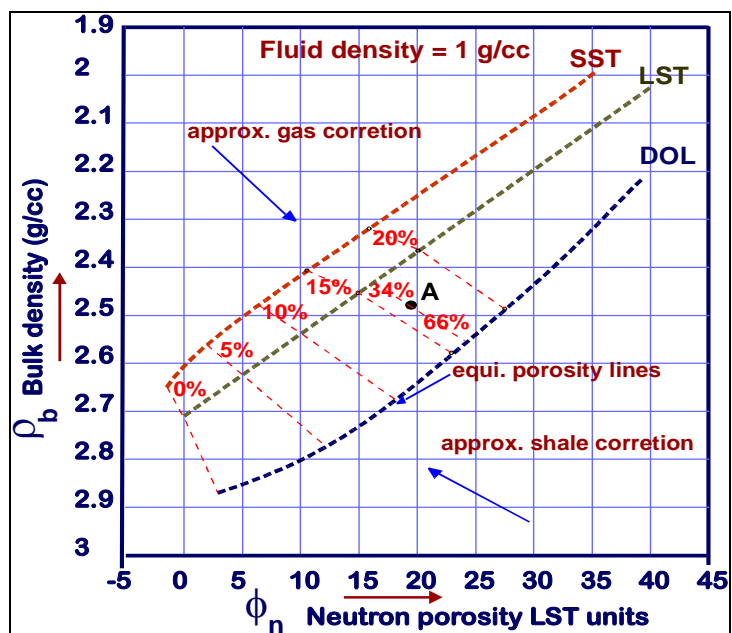

Figure 9A. 5:The density-neutron cross-plot.

9B.2.8.3 SHALY SANDS

In the chapters 5 and 6 the calculation of estimates for the shale volume from respectively the spontaneous potential SP and the gamma-ray log GR were discussed. If the reservoir rock contains a mixture of sand and shale the neutron-density cross-plot can also be used for shale volume calculations. For shaly sands the concept *effective* porosity ϕ_e is defined as :

$$\varphi_e = 1 - V_{sa} - V_{sh} \qquad \text{(eq. 9A.6)}$$

In which V_{sa} is the sandstone matrix volume and V_{sh} the shale volume. This model is the basis of the so-called neutron-density cross-plot (figure 9A.5,6), commonly used to assess ϕ_e and V_{sh} in a shaly formation, whereby the following equations apply:

$$\rho_b = (1 - \varphi_e - V_{sh}).\rho_{ma} + \varphi_e.\rho_{mf} + V_{sh}.\rho_{sh} \qquad \text{(eq. 9A.7)}$$

$$\varphi_n = \varphi_e + V_{sh}.\varphi_{nsh} \qquad \text{(eq. 9A.8)}$$

The method is graphically illustrated in figure 9A.6, for water bearing shaly sand. A triangle is constructed from the clean matrix point ($\phi_n=0$; $\rho_{ma}=2.65$), the 100 % fluid point of water ($\phi_n =100\%$; $\rho_{fl} = 1.0$) and the 100% shale point (ϕ_{nsh} and ρ_{sh}), the latter values are derived from a nearby shale layer. The fluid and shale points are converted to porosities, or; $\phi_{fl} =1,\phi_{sh}=0.5$. The linear effective porosity scale is indicated on the line 100% matrix to 100% water, and also on the 100% shale to 100% water line. Near horizontal lines with the same effective porosity values are drawn between the matrix and shale sides of the triangle. The linear V_{sh} scale is indicated on the matrix-shale side as well as in the shale-water side. Lines with the same V_{sh} values are also drawn. Each data pair (ϕ_n , ϕ_b) entered in this chart produces a value of effective porosity and shale volume fraction.
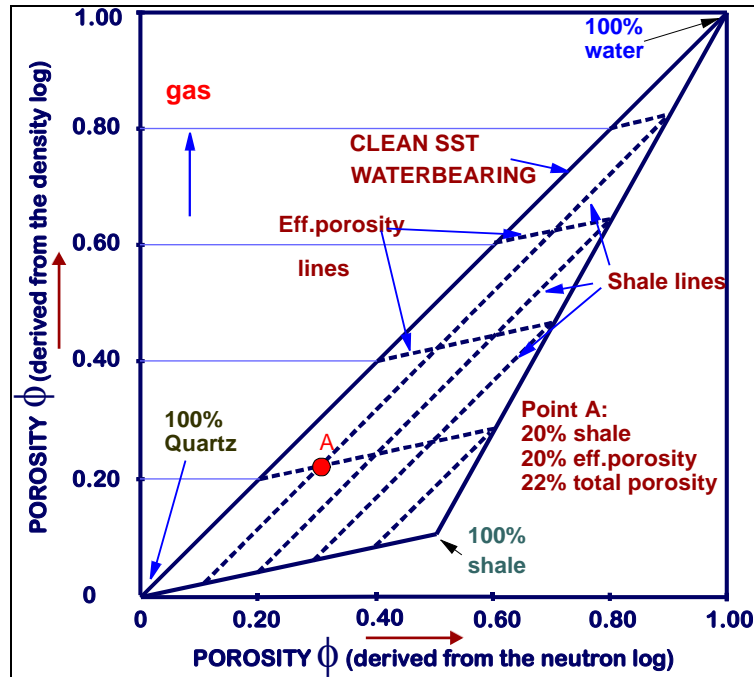

Figure 9A.6: Shale volume and porosity lines in Density-Neutron cross-plot

9B.2.8.4 MULTIPLE MINERAL LOG EVALUATIONS

The unknown matrix volumes and porosities of mixtures of two minerals in a reservoir can be solved with simple matrix algebra. This is possible when the tool responses can be simplified to a set of linear equations. The response of a tool to a mixture of minerals and water is assumed to be the response of the tool to 100% of these minerals multiplied by the volume fractions of the individual minerals. For the density and neutron tool combination three equations can be written accordingly :

- $\rho_b = V_{ma1} \cdot \rho_{ma1} + V_{ma2} \cdot \rho_{ma2} + \phi \cdot \rho_{fl}$ (eq.9A.9)
- $\phi_n = V_{ma1} \cdot \phi_{nma1} + V_{ma2} \cdot \phi_{nma2} + \phi \cdot c$ (eq.9A.10)
- $1 = V_{ma1} + V_{ma2} + \phi$ (eq. 9A.11)

where: dimension

ρ_b	=	bulk density reading log,	g/cc
ϕ_n	=	Neutron bulk reading log, porosity units	%
V_{ma1}	=	Volume matrix mineral 1, fr.b.v.	%
V_{ma2}	=	Volume matrix mineral 2, fr.b.v.	%
ρ_{ma1}	=	matrix density of 100% volume of mineral 1,	g/cc
ρ_{ma2}	=	matrix density of 100% volume of mineral 2,	g/cc
ϕ	=	porosity, fraction of bulk volume	%
ρ_{fl}	=	fluid density, gr/cc	
ρ_{fl}	=	neutron response of 100% fluid, porosity units	%

The known variables, which are based on the log readings, are ρ_b and ϕ_n. The fluid properties are normally based on the mudfiltrate. The mudfiltrate density can be measured on the surface, and the neutron response can be estimated e.g. 1 for 100% fluid. From cuttings the mineral composition is well estimated, so mineral matrix densities can be made. Normally are used; quartz 2.65 g/cc, dolomite 2.87 g/cc and limestone 2.71 g/cc. The unknowns are the matrix volumes V_{ma1}, V_{ma2} and porosity ϕ.

Then three equations with three unknowns can be solved. With the three porosity tools and the photo-electric absorption coefficient P_e many combinations can be made to obtain three equations with three unknowns. The equation for a Sonic - Pe combination is as follows:

- $\Delta T = V_{ma1} . \Delta T_{ma1} + V_{ma2} . \Delta T_{ma2} + \phi . \Delta T_{fl}$ (eq. 9A.12)
- $P_{eb} . \rho_b = V_{ma1} . U_{ma1} + V_{ma2} . U_{ma2} + \phi . U_{fl}$ (eq. 9A.13)

Where :   dimension

ΔT	=	sonic log reading,	$\mu s/ft$
ΔT_{ma1}	=	sonic log reading 100% matrix mineral 1,	$\mu s/ft$
V_{ma2}	=	sonic log reading 100% matrix mineral 2,	$\mu s/ft$
ΔT_{fl}	=	sonic log reading 100% fluid,	$\mu s/ft$
P_{eb}	=	photoelectric absorption cross section of the formation	barns (1 barn = 10^{-24} /atom)
ρ_b	=	bulk density formation, g/cc	
U_{ma1}	=	volumetric eff. photoelectric abs. index of mineral 1,	barns/vol
		$U = P_{eb} . \rho_b$ in which ρ_e stands for the electron density	
U_{ma2}	=	volumetric eff. photo electric abs. index of mineral 2,	barns/vol
U_{fl}	=	volumetric eff. photo electric abs. index of fluid,	barns/vol

The logical extension of this evaluation scheme is the incorporation of more log readings from other tools. However incorporating more equations can lead to an over-determined system, with more equations than unknowns. Computer programmes have been constructed based on least squares algorithms that solve sets of tool response equations for porosity, mineral & shale volume fractions, taking into account the error bars of the measurements, and the constraints of the equations by means of weight factors. These evaluation methods will be discussed in the third year lectures.

9B.2.9 SATURATION DETERMINATION FROM LOGS

In chapter 5 the Archie equations were discussed :

$$C_t = \Phi^m . S_w{}^n . C_w$$ (eq. 9A.14)

The cementation factor m and saturation exponent n, are usually estimated to be 2 due to the absence of core analyses. If information on the consolidation of the reservoir rock is available, the m,n-lithology tables in chapter 5 can be used to refine this estimate. The conductivity C_t and the porosity ϕ are measured with well logs, while the formation water conductivity C_w is obtained from the analysis of produced water samples or can be derived from the SP log. For the latter an accurate analysis of a representative mud-filtrate sample is required to estimate the mud-filtrate conductivity C_{mf}.

$$E = (-71).log \frac{C_w}{C_{mf}}$$
(eq. 9A.15)

If the reservoir extends into a water zone ($S_w =1$) equation 9A.15 can be rearranged as :

$$C_w = C_t / \phi^m,$$
.
(eq. 9A.16)

In this way a reliable estimate of the formation water conductivity C_w is obtained. An additional advantage of deriving C_w from a water-bearing zone is that errors in estimating the cementation factor "m" and C_w are partly compensated.

Remember that the effect of the clay conductivity in shaly sands can have a large disturbing effect on the determination of water saturations with the Archie and the Humble equations.

9B.2.10 FLUID CONTACTS

Knowledge on the in-situ present fluids is essential to identify:
- the reservoir fluid type,
- the spatial characteristics in the reservoir (vertical presence),
- reservoir flow characteristics
- fluid transport characteristics in the production well.

9B.2.10.1 WIRELINE FORMATION TESTING

Wireline logs can give indirect indications on the fluid type that occupies the pore space, however the acquisition of physical samples is often required to solve unclear wireline log interpretations. Moreover, when the reservoir layer, which is penetrated by the well, contains only a part of the total oil column, pressure data are required to identify the oil water contact. In the sixties the formation tester was introduced, which consisted of a sample chamber and a pad in which a shaped charge was embedded. The pad was

Figure 9A. 7: Operation of the RFT tester probe (After Schlumberger)

pressed (set) against the borehole wall and the perforating charge was then used to establish communication between the reservoir and the sample chamber via a flow line. In the seventies a nozzle that could be extended through the mudcake into the reservoir replaced the perforating charge. An example of this tool type is the repeatable formation tester or "RFT" of which the principle is depicted in figure 9A.7. In contrast with its predecessor, the RFT is limited to measuring formation pressure and to retrieving formation samples in open holes only. The flow-line that connects the nozzle or probe to the chamber contains a number of valves that allow multiple settings of the tool and
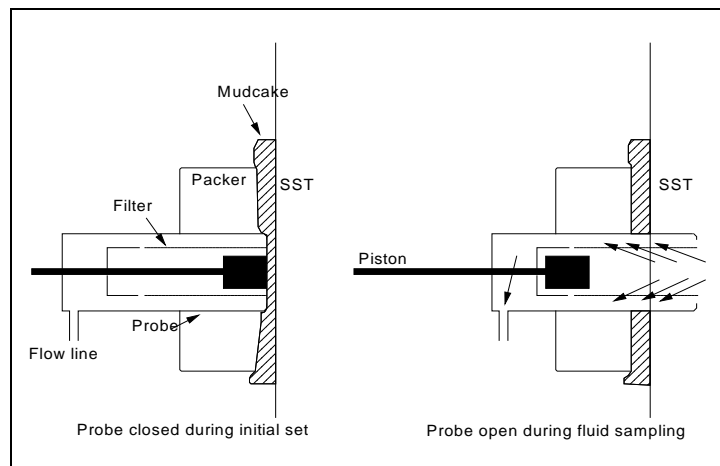
collection of several formation fluid samples. At each setting the pressure of the reservoir fluid can be measured with a strain gauge or a quartz high-resolution pressure gauge.

In the eighties the modular formation tester or "MDT" was introduced. It has two or three sampling probes and measures vertical permeabilities based on the propagation of a pressure sink from one probe to the other positioned higher up in the hole. Running a GR or a SP with the wireline test tool can control the accuracy of the setting of the test tools at a certain depth. Correlation of these GR or SP logs with open hole SP or GR curves gives the desired depth control.
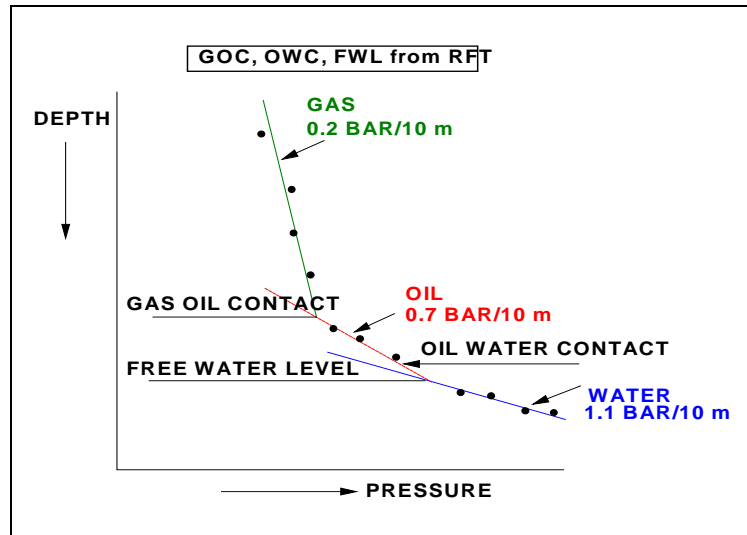
Figure 9A. 8: Fluid contacts that can be obtained with fluid pressure measurements.

The reservoir pressure measurements plotted against the depth will produce a gradient that is very steep for gas, much flatter for oil, and has the smallest angle for water. The pressure measurements are used to detect gas/water, gas/oil or oil/water contacts based on the recorded fluid gradient (figure 9A.8).

9B.2.10.2 LOG SATURATION PROFILES AND CAPILLARY PRESSURE CURVES
The water saturations derived from resistivity logs give accurate information on the saturations of individual layers. However, they are surprisingly unreliable in isolation to determine the hydrocarbon water contacts. This is due to the very gradual transition from some 85% water to 100% water saturation that occurs in most reservoirs. Moreover, the free water level (FWL), defined as the level where the capillary pressure is zero, can be several meters lower than the depth where the logs give 100% water saturation (chapter 4, capillarity)

If capillary pressure curves, measured on core samples, are available, then a direct comparison between water saturations, derived from logs and from capillary pressure curves, can be made. An example is shown in figure 9A.9. If the saturation profiles of the two data sources are depth matched a more reliable estimate of the free water level (FWL) can be made even when the log derived saturation profile does not extend to the water table.
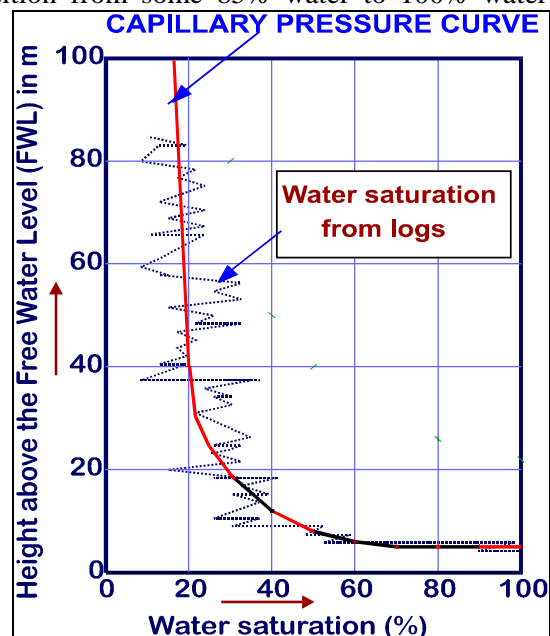
Figure 9A. 9: Comparison log-derived and cap-curve derived saturation profiles

9B.2.11 HYDROCARBON RESERVES VOLUME ESTIMATION

The Hydrocarbon-Initially-In-Place is the product of bulk reservoir volume, net/gross ratio, effective bulk porosity, initial hydrocarbon saturation, and hydrocarbon formation volume factor :

$$HCIIP = V_b . N/G . \varphi . S_{hc} . \frac{1}{B_o} , \qquad \text{(eq. 9A.17)}$$

where   dimension:
HCIIP   =   Hydrocarbon-Initially-In-Place m^3
V_b =   Gross Rock Bulk volume m^3
N/G   =   Net over Gross ratio   d.l.
ϕ =   Porosity, fraction of bulk volume   fraction
S_{hc} =   initial Hydrocarbon Saturation, fraction of pore volume   fraction
B_o =   Initial hydrocarbon Formation Volume Factor   d.l.

The B_o factor converts the volume of oil under reservoir pressure and temperature conditions to the conditions on the surface. The B_o factor comprises the shrinkage and gas expansion. The recoverable reserves are defined as :

$$recoverable\ reserves = HCIIP . RF \qquad \text{(eq. 9A.18)}$$

The Recovery Factor RF indicates what fraction of the original oil volume that is present in the reservoir, is eventually expected to be brought to the surface. RF can vary from more than 50% for a reservoir with a very strong natural water drive, to less than 10% for tight carbonate reservoirs with very little natural drive energy. With enhanced oil recovery in the form of water injection, gas injection, polymer or CO_2 flooding, the RF factors can be increased very significantly.

The product   h. Φ. S_{hc} , in which "h" is the net reservoir thickness, and "S_{hc}" is the hydrocarbon saturation, is called the hydrocarbon column. The generation of this column is shown in figure 9A.10 and it is further discussed in the following example.
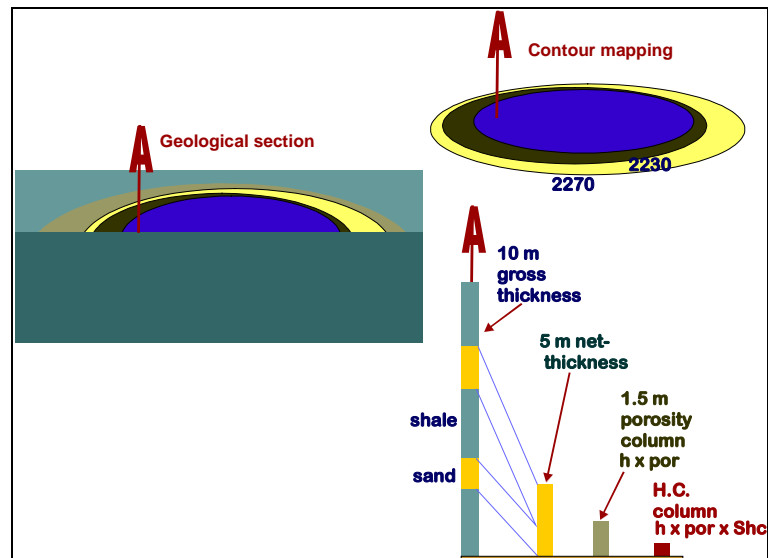
Example:
The interval consists of shales alternated with oil-bearing sandstones. The sandstones have an average porosity of 30 % and an average oil saturation of 67 %. The

Figure 9A. 10: Generation of a hydrocarbon column

gross interval of 10 m in our example refers to the total interval including non-reservoir sections. The net interval refers to the cumulative reservoir thickness and amounts to 5 m. Compressing the 5 m net reservoir with an average porosity of 30 % results in 3.5 m of massive (0 % porosity) rock and a 1.5 m **porosity column** (with 100 % porosity). The porosity column is filled for of 67 % with oil which is equivalent to 0.67x1.5 = 1 m **oil column** and a 0.5 m water column.

9B.1 GENERAL INTRODUCTION ON THE EVALUATION OF COAL AND WATER

In this B-section of chapter 9 the evaluation of wireline log information is continued for coal and groundwater. As mentioned in the general introduction, chapter 1, impressive progress was made during the last decade in the interpretation of geophysical measurements. Direct coal, ore, hydrocarbon or groundwater indicators can frequently be derived from surface seismic, provided accurate well data over the area of interest is available for calibration. For exploration and appraisal activities direct physical contact with the prospective layers is even now required to resolve the question whether profitable occurrences are present. In Chapter 3, committed to various methods of formation evaluation, the analysis of drill cuttings and cores was discussed. These methods are common for the four petrophysical application areas, which are covered in these lectures:

- hydrocarbons,
- coal,
- groundwater, and
- minerals and/or mechanical properties.

Again, this section 9B will concentrate on the analysis of wireline logs to determine the water quality and coal quality, as listed in table 9B.1.

LOCATE:	Target seam or reservoir and
DETECT:	Fluid, gas, non-HC content
EVALUATE:	lithology porosity permeability capillary properties mechanical strength salinity of the water original gas saturation movable hydrocarbons residual hydrocarbons % oil / gas / water gross / net thickness reservoir pressure

Figure 9B. 1: Objectives of a petrophysical interpretation.

9B.2 EVALUATION OF COAL SEAMS

9B.2.1 INTRODUCTION & HISTORY

The developments in the theory of rock physics originally started, as mentioned in chapter one, with the applications for ore and coal exploration or exploitation. Uncomplicated electric, and (electro-) magnetic techniques and degasification/exploration- drilling in advance of the worked coal seams, were good examples for petroleum and water exploration. After a period of (economic) stagnation, the development of logging tools for coal, ore, and ground-water evaluation was supported for three reasons:

1. The conventional method of drilling large core holes to obtain samples for laboratory analysis became progressively more labour intensive and more costly.
2. Deeper and more complex deposits were explored, which justified the use of geophysical techniques.
3. Probably the most important reason; Slim-line logging tools with a diameter of only 1 to 2 inches were developed. These tools not only fitted in the slim holes used for coal and mineral exploration. They also provided standard services with the same accuracy as their big brothers (3-5 inch diameter), which were used up till then in the oil industry. The UK based company BPB Wireline Services is the market leader in the slim-hole logging business, and this chapter is based on training material provided by that company[1].

Due to the cost cutting drive, initiated by the long period of low oil prices, slim-hole drilling is at present frequently used. As a result the slim-tools have been upgraded to withstand the high pressures

---

[1] The contribution by BPB and their commercial manager Dr. P. Elkington is gratefully acknowledged.

and temperatures that are frequently encountered in oil wells. Most wireline services can now be provided in 3-inch holes with the current (1995) tools. Exceptions at the time of writing are fluid sampling tools and borehole micro-resistivity imaging devices. **The principles of the tools used for coal logging are the same as their counter parts used for the oil industry. Therefore, the principles will not be repeated and the reader is referred to the chapters 3 to 8.**

In the next sections the determination of the coal quality parameters from wireline logs will be discussed. It is emphasised that in the same way as for oil reservoir analysis, empirical relations are required between the physical properties that we can measure (natural gamma-radiation, electron density, neutron absorption, resistivity) and the parameters that we want to know (ash, moisture, organic matter). These relations are also equivalent to their oil-cousins in the sense that they are often only valid in one basin or even one coal deposit.

9B.2.2 COAL QUALITY

For coal exploration and appraisal it is of utmost importance to determine the coal quality at a very early stage in the development. The coal quality can be determined when the following properties are known:

a) the ash content
b) the moisture content, and
c) the fixed carbon content.

Ad. a:
The ash content is defined as the residue that remains after the coal is burnt.

Ad. a, b and c:
Commercial coal classification is usually based on the "so called" proximate analysis. This analysis involves the measurement by weight of the successively gassified coal fractions, when the temperature of a sample is raised till all the coal is burnt. These fractions are:

- labelled inherent moisture,
- volatile matter,
- ash, and,
- by mass balance the fixed carbon content.

It will be evident that the volume fractions of ash, moisture and coal, which determine the coal quality, are closely related to, but not identical to, the weight fractions of the proximate analysis (ash, moisture, volatile matter, and fixed carbon). The ultimate analysis is basically an accurate chemical analysis of the coal and determines, amongst others, the amounts of carbon, hydrogen, nitrogen, and oxygen.

Coals can be classified according to their degree of coalification or rank, which ranges from lignite to anthracite. Broadly speaking the ash content is more important for bituminous and higher rank coals, whilst moisture becomes more important for sub-bituminous and lignitious (brown) coals.
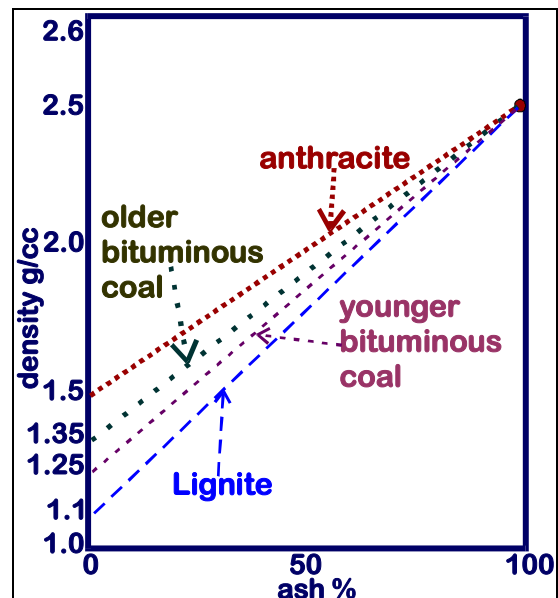
Figure 9B. 2: The density of coal related to ash content.

9B.2.3 ASH CONTENT

Depending on coal rank, the ash content of a coal will generally increase with density. The end-points of this linear relation are the weight of 100% pure coal and 100% ash, as shown in figure 9B.1. The last point represents the density of sediment (2.65 gr/cm^3) while the previous depends on the rank of

the coal. It varies from 1.1 gr/cm^3 for lignite, via 1.3 gr/cm^3 for bituminous coal, to 1.5 gr/cm^3 for anthracite. It is emphasised that the relations shown in figure 9B.1 are only estimated and that ash and clean coal densities measured on actual coal samples are required to apply this relation with confidence.

$$\rho_{bulk} = \rho_{ash} \cdot V_{ash} + \rho_{carb} \cdot V_{carb} \qquad \text{(Eq. 9B.1)}$$

The carbon volume is referred to as V_{carb}, and the ash volume as V_{ash}, while carbon density (100%) is referred to as ρ_{carb} and the ash density (100%) as ρ_{ash}.

Equation 9B.1 and the parameters for ash and clean coal can be entered in a well-site computer and used for an on-line display of the ash content alongside the density log(s). An example is shown in figure 9B.2. The logs in this example are automatically blocked to simulate the layered character of the subsurface, taking into account the inflection points of the various log responses. It should be realised that that the coal layer thickness is often a very critical parameter. An ash streak of only one decimetre thickness or a low quality coal streak can make the difference between economic exploitation and a marginal development. The resolution of conventional density logs is restricted to about 45 cm. Special high-resolution density tools like the bed resolution density tool (BRD) from BPB were developed to detect coal bed boundaries with an accuracy of 15 cm.
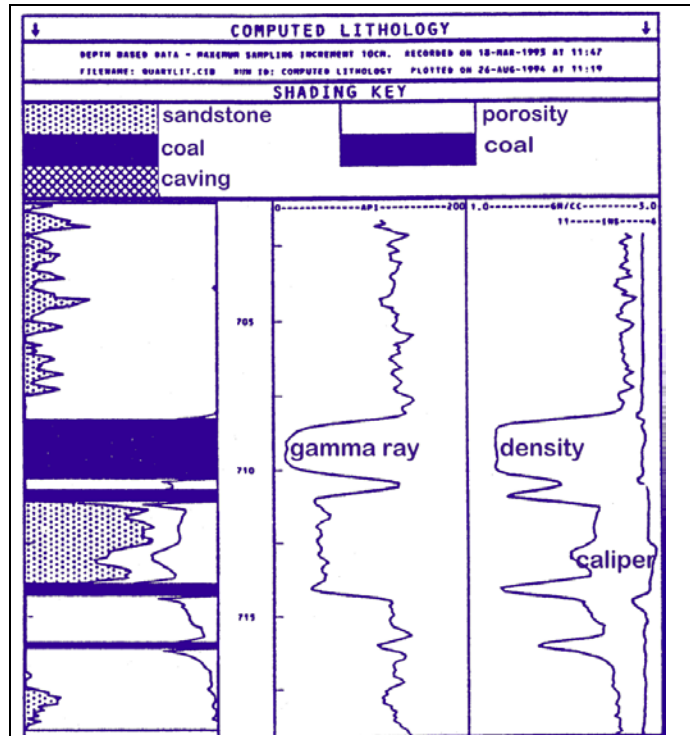

Figure 9B. 3: Computed Lithology Analysis derived from log data

9B.2.4 MOISTURE CONTENT

Due to the low permeabilities of the coal and the absence of a continuous pore network the resistivity logs are usually not suited for water saturation determination. However, the evaluation scheme presented for ash and clean coal can be extended with moisture if more logs are taken into account. Lithology and porosity (moisture content) is then computed from a set of linear equations with the following parameters:

- sonic, and density log readings
- matrix response of the minerals for sonic, and density tools

If the coal is assumed to consists entirely of carbon, ash, and moisture (porosity), then the following set of equations can be formulated:

$$\Delta T = \Delta T_{fl} . V_{mois} + \Delta T_{ash} . V_{ash} + \Delta T_{carb} . V_{carb} \qquad \text{(eq. 9B.2)}$$

$$\rho_b = \rho_{fl} . V_{mois} + \rho_{ash} . V_{ash} + \rho_{carb} . V_{carb} \qquad \text{(eq. 9B.3)}$$

$$1 = V_{mois} + V_{ash} + V_{carb} \qquad \text{(eq. 9B.4)}$$

Here the carbon volume is referred to as V_{carb}, the ash volume as V_{ash} and the moisture volume as V_{mois}. Then the carbon transit time is ΔT_{carb}, the ash transit time as ΔT_{ash}, and the moisture transit
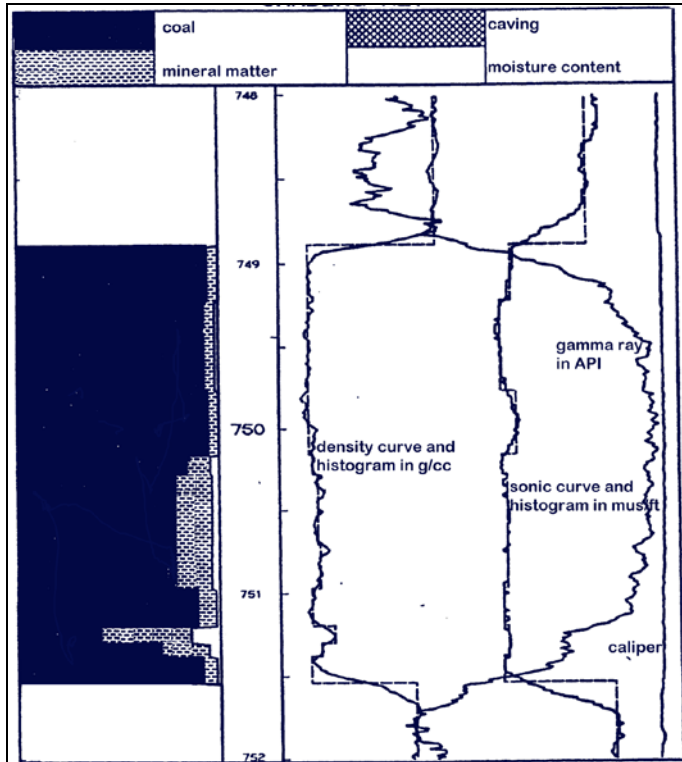
Figure 9B. 4: GR, sonic and density log, with the ash, moisture and coal fractions.

time as ΔT_{mois}. Finally the carbon density (100%) is ρ_{carb}, the ash density, ρ_{ash}, the moisture density ρ_{fl}.
With 3 equations the 3 unknowns V_{ash}, V_{carb} and V_{mois} can be determined. The results of a computer evaluation that uses this scheme and the original logs are depicted in figure 9B.3.

9B.2.5 FLOATS/SINKS, CALORIFIC VALUE, VOLATILES, SULPHUR

Coal samples are often not only tested to find the proximate analysis results but also to find out whether the quality of the coal can be improved by gravity separation. In this method the grinded coal is dumped into a bath that contains a fluid with a density between the ash (heavy) and the coal (light) densities. The coal floats and is skimmed from the fluid surface. Making a histogram of the num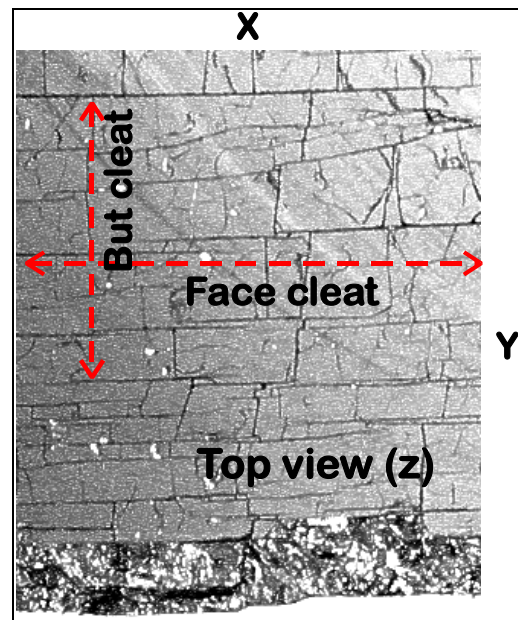ber of layers with a certain density vs. the density itself can simulate this process. The most effective density of the separation fluid can then be determined by plotting this density in the histogram.

Other coal quality parameters, such as calorific value and volatiles content have been successfully predicted from logs in many instances. However in contrast to the relations derived in the previous sections, which are at least based on physical phenomena, the relations for calorific value and volatiles content are entirely empirical, and can only be established if sufficient measurements of these parameters on coal samples are available.

Another very important parameter, the sulphur content, cannot be determined with the conventional coal-logging suite of tools. However sulphur content can be determined with the slim-line (1 11/16") pulsed neutron tool. Neutrons with high energies (14 MeV) can activate nuclei during inelastic collisions. When fast neutrons collide with sulphur atoms gamma radiation with a very characteristic energy of 3.4 MeV is emitted. The gamma radiation can be sorted in an energy spectrum (see chapter 6). The height of the sulphur peak in the spectrum is a measure for the sulphur content of the coal. Although this method is promising the relatively high cost of the pulsed neutron logging survey has till now prevented commercial application in the coal industry.

Photo 9.B. 1: Carboniferous coal, Beringen - Belgium: Top view with the lateral running main cleat systems.

9B.2.6 COALBED METHANE

Recent years have seen an upsurge in the exploration of coal for its gas content. In underground mines the methane released by the seams at the coalface is a severe hazard. Strict safety measures (mine lamps, pneumatic tools, explosion free electric lights), and extensive ventilation were required to minimise the risk of explosions. With the emergence of horizontal drilling techniques, and advances in geo-steering of the drill string, which ensure that the hole trajectory remains within the coal seam boundaries, it became at least technically feasible to drill a number of methane producing holes in a coal deposit. However the economic viability of these ventures has been marginal despite hefty tax incentives in the USA. Nevertheless research projects are currently under way to investigate the suitability of methane production from shallow coal deposits in the USA and in The Netherlands.

Figure 9B. 5: Comparison of the core and log derived methane gas content

In addition to the usual parameters such as bed thickness, ash-, moisture-, fixed carbon content one would like to derive the porosity, cleat- and micro-permeability, and formation pressure from logs, in order to determine the productivity of the coal seams.
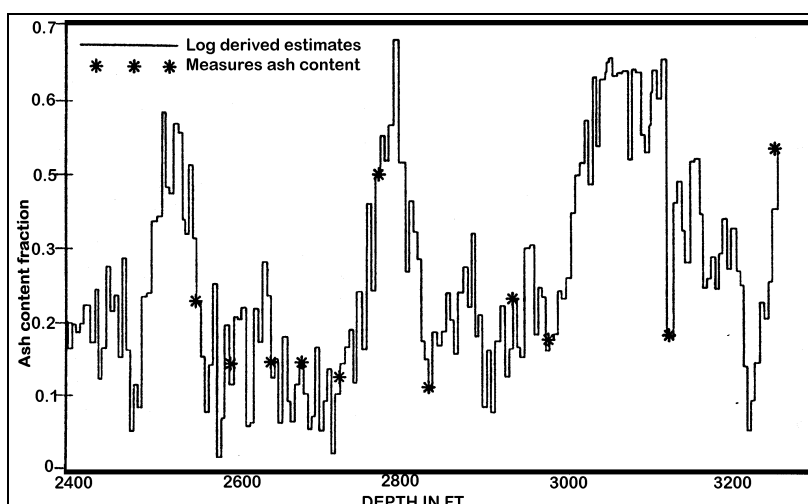
Figure 9B. 6: Comparison of core and log derived ash content

Due to the very low cleat porosity (1-2 %) and higher micro-pore porosity (~ 8 %) and permeability (< 0.1 mD range) this only can be achieved indirectly by relating these parameters to other log measurements. It has been possible to relate the gas content to the ash content for certain coal basins. An example is given by M. Mavor SPE Formation Evaluation Journal 12/94:

$$V_{gas} = a - b. V_{ash}$$

(eq. 9B.5)

In which V_{gas} is expressed in cft/ton or m^3/kg and Vash as a volume fraction. The ash content is in this case derived in the same way as shown in equation 9B.1, which relates the ash content directly to the bulk density and ignoring the effect of the moisture. The ash content prediction is shown together with core derived values in figure 9B.1. The coefficients a & b of equation 9B.3 are also found from core analysis. It is emphasised that this method, contrary to the ash content determination, is very much dependent on the coal properties of a particular basin, and should always be calibrated with core data.
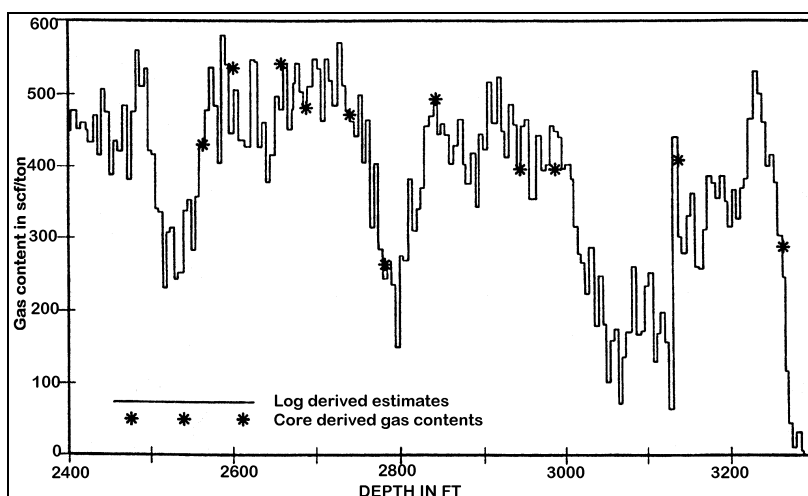
Coal gas-content, is reasonably good to estimate (figure 9B.4). Especially for the coal mining industry and its firedamp problems, the methane content is always estimated as good as possible. It was also attempted to relate the gas permeability to the water saturation of the pore system of the coal. The gas is however mainly conducted by the micro-fracture network in the coal (cleats) which is very difficult to describe with oil-industry methods. Coal with a modest ash fraction (sandstone) proved to be a better methane conductor than clean coal that contained a higher gas content, but was less permeable. It is concluded that for permeability and productivity prediction core analysis is indispensable, and that relations that predict permeability on a milliDarcy-level (µD) should be used with a lot of caution.

9B.2.7 LIGNITE (BROWN) COAL

Mining of brown coal is often associated with less developed economies (former East Germany, Poland) or countries with plenty of open spaces like Australia. However in Western Europe in a densely populated area between Köln and Aachen, very extensive open cast mines are in operation. In these mines brown coal deposits of the lower Rhine basin are excavated. Brown coal has a very low rank, a very high moisture content, and consequently a low calorific value. This "compressed peat" is mainly used to fire power stations hence the quality of the peat has to be very constant. This to avoid troubles with the furnaces, which cannot cope with too much moisture or too much ash. The Rhein Braun company that mines the lignite makes extensive use of wireline logs not only to assess the position and quality of the coal, but also for an accurate determination of the thickness and mechanical properties of the overburden. In figure 9B.6 an example of a logging suite run over the brown coal is shown together with a geological interpretation. The combination of low gamma-ray log and a low-density log readings is an excellent indicator for the presence of brown coal. In contrast with the hard coal the resistivity recorded over brown coals can at least give a qualitative indication of the moisture content, and therefore of the coal quality.
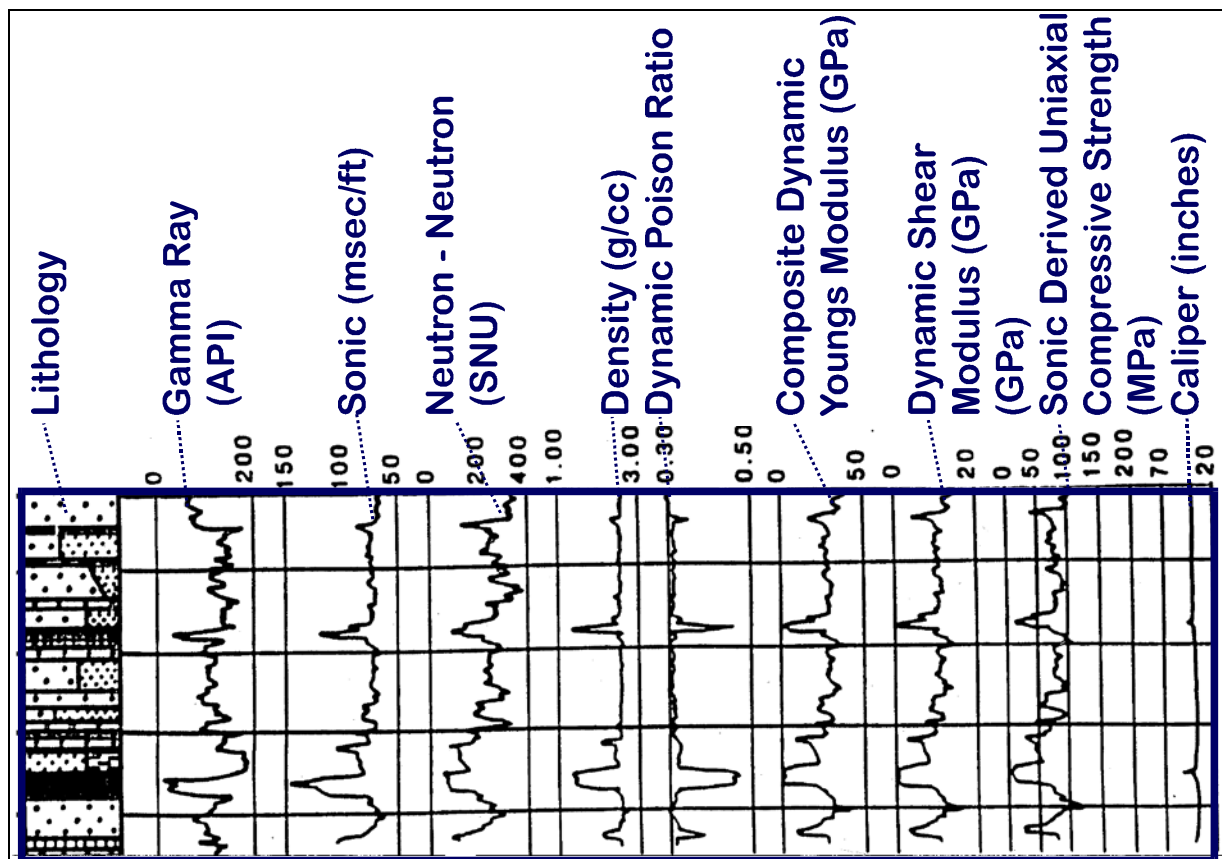

Figure 9B. 7: Example of a coal log evaluation, using the regular tools and the derived rock strength parameters (sonics)

9B.3 EVALUATION OF GROUNDWATER

9B.3.1 INTRODUCTION AND HISTORY

Although the drilling of water wells has a much longer history than the drilling of oil wells, wireline many of the rock physical concepts for log evaluation were adapted and used after the logging techniques have been developed and commercialised for the oil industry. This development is not surprising if one considers that a deep water well will cost at most a few hundred thousand guilders, while even a relatively shallow oil well (1500 m deep West of Holland) still cost more than 5 million guilders. The funds that are available for the evaluation are of course related to the total investment, hence the budget for water well evaluation has traditionally been modest, and only simple tools could be used for the surveys. This situation is even more complicated due to the fact that nuclear tools with chemical radioactive sources cannot be used in water wells for health and environmental reasons. If a source is lost not only would the hole have to be abandoned but also the entire potable water producing aquifer could be in jeopardy!

Despite these limitations Dutch Institutes involved in the survey of the shallow subsurface like the Groundwater Survey of TNO-NITG adopted wireline logging already in the fifties. They perfected their own logging tools and interpretation methods. They provide important information on the lithology, water quality and inflow performance of the water wells. TNO has several small logging trucks with tools that are used to log water wells on a daily basis. They are equipped with resistivity, natural gamma radiation and spinner logging tools. This Chapter is a summary of documentation provided by the TNO-NITG (Drs. van Overmeeren), whose contribution is gratefully acknowledged. The technical information provided by Welenco, an industry leader in shallow slim well logging in the volume on Water & Environmental Geophysical Well Log, is also extensively used in this section.
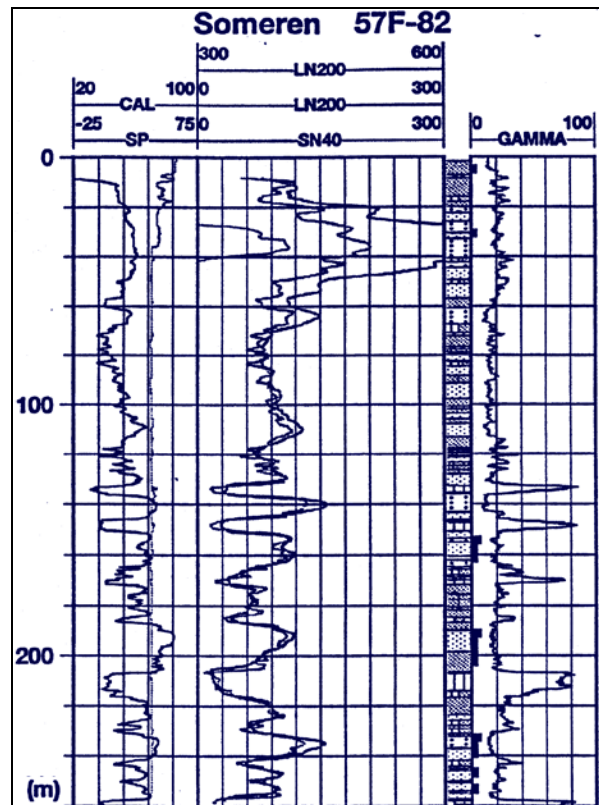

Figure 9B. 8: An example of an open hole logging survey.

9B.3.2 LOGGING TOOLS IN OPEN WATER WELLS: METHODOLOGY

A standard logging survey in an open water well usually consist of:
- the short-normal (SN) & long normal (LN) resistivity tools,
- a spontaneous potential (SP) tool,
- a natural gamma-ray (GR) tool, and,
- a calliper (ϕ) tool.

The tool diameters are usually between 1 to 2", and the surface equipment is often mounted in a van or small 4 wheel. Till the mid-80's water well logging and interpretation was usually restricted to a multi-pen log plot. Evaluations were done with a programmable pocket calculator. With the development of powerful PC's and laptops for data-acquisition, registration, interpretation and storage, the wellsite computers became standard since the early nineties. An example of an open hole logging survey is shown in figure 9B.7. Here SN40 and LN200, the numbers in the tool mnemonics (header), give the distance between the measuring electrodes of these tools in cm. The measuring electrode spacings are standard for small diameter holes. For holes with larger diameters spacings,

sometimes up to 200 cm, are used. All tools have a small diameter of 5 cm or less. The details of the normal resistivity tools are found in chapter 5, while the SP and GR are covered in the chapters 6 and 7 respectively.

9B.3.3 PARAMETERS REGARDING THE CONDITION OF WATER

The following water quality terms:
- Salinity, or the total dissolved solids (TDS),
- chlorine or the content of Cl⁻ ions, and,
- hardness,

all use the concentrations of one or more of the ions that are dissolved in the water, to characterise the water quality.

The TDS is based on the ratio of the weight of dissolved solids and the volume expressed in mg/l. TDS and corresponding chlorine contents Cl⁻ in ppm (part per million) are listed in table 9B.1. The chlorine content is in turn related to the conductivity. The table implies therefore a relation between the water conductivity C_w

Figure 9B. 9: Water salinity versus resistivity (here given in ρ_w instead of R_w)

expressed in mS/m (milli-Siemens per meter) and the TDS in mg/l, which can be expressed as:

$$TDS = 7 * C_w$$
(eq. 9B.6)

However the proportionality constant varies between 5.5 and 7.5, depending on the type of ions that are present in the water. As shown in figure 9B.8, the presence of bicarbonates, or HCO_3^-, leads to variations at low Cl⁻ amounts. In this graph the water resistivity ρ_w (Ohm.m) is plotted instead of the conductivity C_w (mS/m). ρ_w is

	TDS mg/l	chlorine content Cl⁻ ppm
fresh water	< 1,000	< 150
brackish water	1,000 - 10,000	< 10,000
salt water	10,000 - 100,000	> 10,000
Brine	> 100,000	

Table 9B. 1 Relation total dissolved solids and chlorine content

the inverse of C_w divided by 10^3. As in the oil industry the equations involving conductivities or resistivities are only valid for a certain reference temperature "T_o". The following relation is used to convert conductivities "C_w" made at different temperatures T to standard conditions C_o and T_o:

(eq. 9B.7)

$$C_w = C_o (1 + 0.0226*(T - T_o))$$

This conversion is equivalent to the temperature corrections discussed in chapter 5 when the Archie equations were derived. The water resistivity ρ_w *(called R_w in the rest of this section)* can also be calculated from the NaCl concentration of the water. For solutions that contain significant ion concentrations, other than Na⁺ and Cl⁻-conversion factors, have to be applied as shown in figure 9B.9. Typical values for water resistivities as they occur in nature are depicted in figure 9B.10.
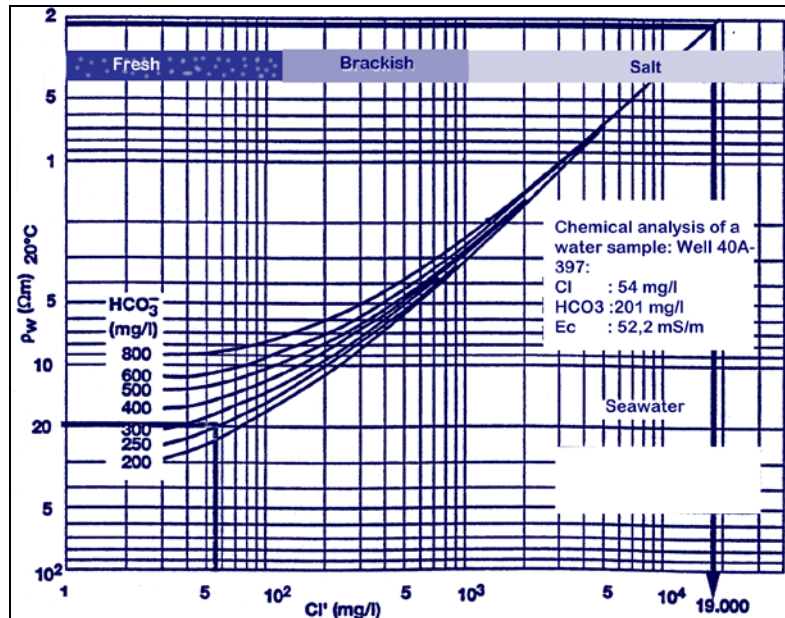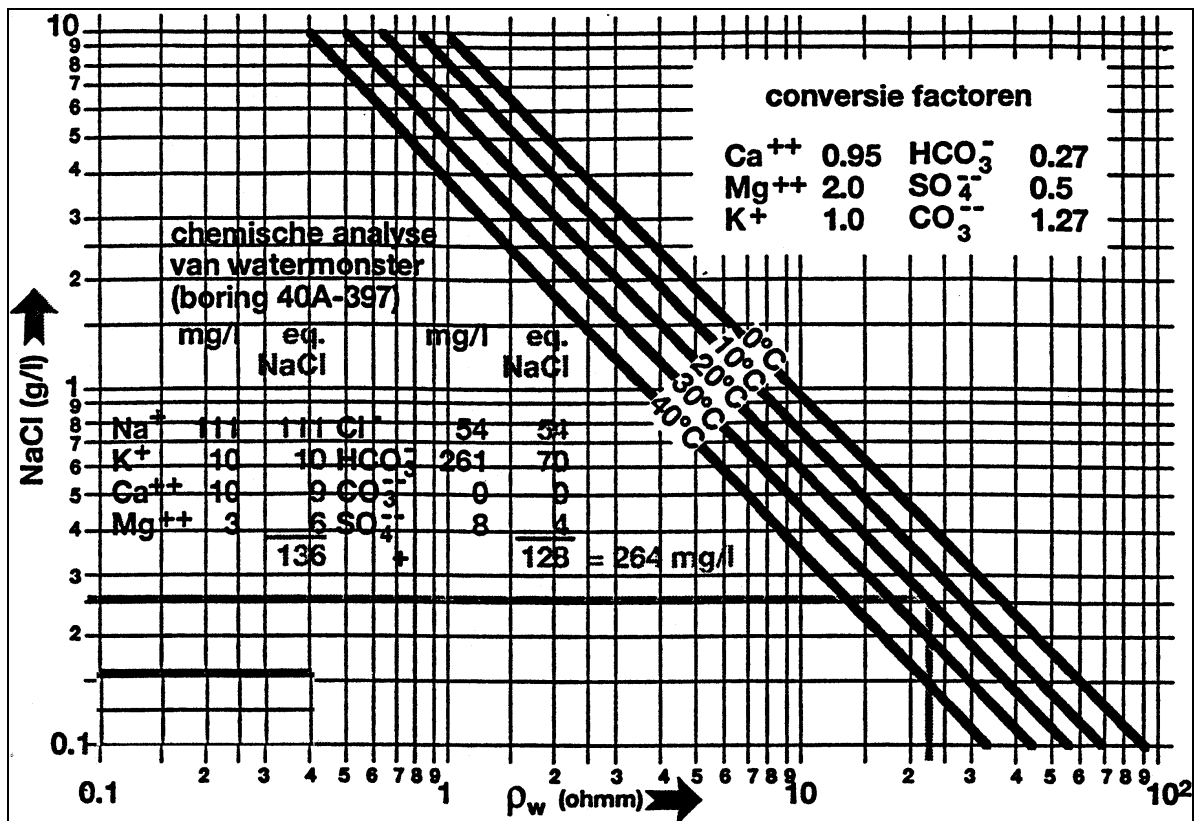
Figure 9B. 10: Conversion factors for ions to resistivities in Na-equivalents at different temperatures.

Hardness H appears to be a nationalistic unit as the definition varies from one country to the next :

German degrees : $H (^oD) = 0.14 * Ca^{++} (mg/l) + 0.231 * Mg^{++} (mg/l)$ (eq. 9B.8)

English degrees : $H (^oE) = 100 * CaCO_3 (grains / gallon) \sim 0.80\ H (^oD)$ (eq. 9B.9)

French degrees : $H (^oF) = 100 * CaCO_3 (mg/l) \sim 0.56\ H (^oD)$ (eq. 9B.10)

In The Netherlands the German definition is commonly used.

Aquifers used for drinking water usually have low concentrations of Cl^- ions (< 50 ppm). For these low NaCl-concentrations the water conductivity is dominated by Ca^{++} and Mg^{++} concentrations, and a relation between hardness H and conductivity C or ρ or σ expressed in µS/cm can be established as shown in figure 9B.11.
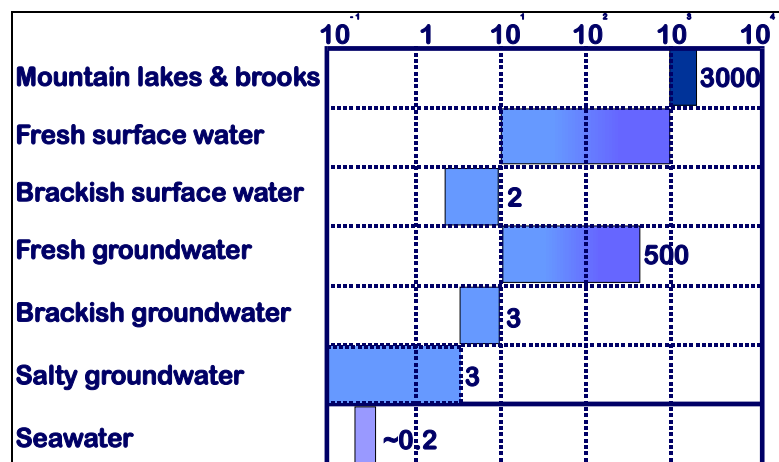

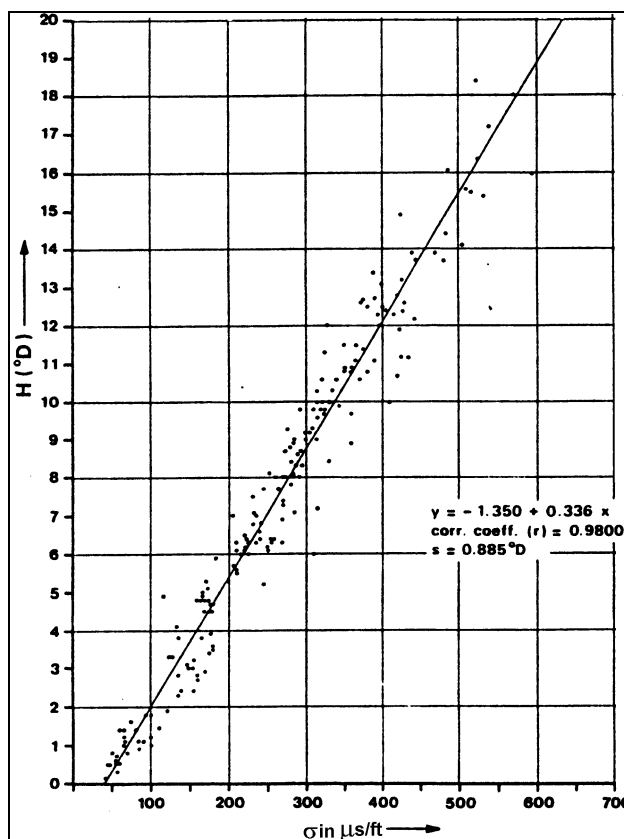Figure 9B. 11: Resistivities of different water types

Figure 9B. 12: Relation between hardness H and conductivity σ.

LOCATE:	aquifer position
	fresh / salt water interface
	impervious layers
EVALUATE:	lithology
	porosity
	permeability
	salinity of the water
	hardness of the water
	shaliness
	total dissolved solids
	grain-size / sorting
	gross/net thickness
	aquifer pressure

Table 9B. 2: Objectives of water well log interpretation.

9B.3.4 THE INTERPRETATION OF LOG INFORMATION

9B.3.4.1 GENERAL ASPECTS

The interpretation of wireline logs run in water wells should ideally give information on all the parameters listed in table 9B.2. However, as usual in nature, physical and chemical properties of the sediments and fluid sometimes disturb the required readings already before interpretation. Here common use of relations and interpretations are discussed. The exceptions are presented in a later stage of your educational programme.

9B.3.4.2 AQUIFER POSITION & NET OVER GROSS

The gamma-ray (GR) and spontaneous potential (SP) logs are applied to distinguish sand and shale layers, using interpretation schemes that are identical to the oil-field procedures earlier described in chapter 6. Likewise these logs are also used to determine the net over gross ratio. An important factor to consider is that the SP changes polarity, when the logging tools travels from a fresh to a salt water bearing formation. It is assumed that the bore hole fluid salinity remains approximately the same during this traverse. Although this polarity change is a strong indication for a boundary between fresh and salt water, without collaboration from other log readings, it can give misleading information on the position of the sand and gravel layers that from the aquifers.

In contrary to oil-field experience, the salinity in water wells can change from a few 100 ppm NaCl to the sea water level of 30,000 ppm within a depth interval of only a few meters (see chapter 2 and figure 9B.10). All logs should therefore be taken into account to determine the net intervals. This situation is made more complex by the fact that in water wells thick mud-cakes are an exception. The invasion of the permeable layers is therefore often not controlled and invasion of drilling fluid can be so deep, or mixed up with the original water, that a SP is suppressed.
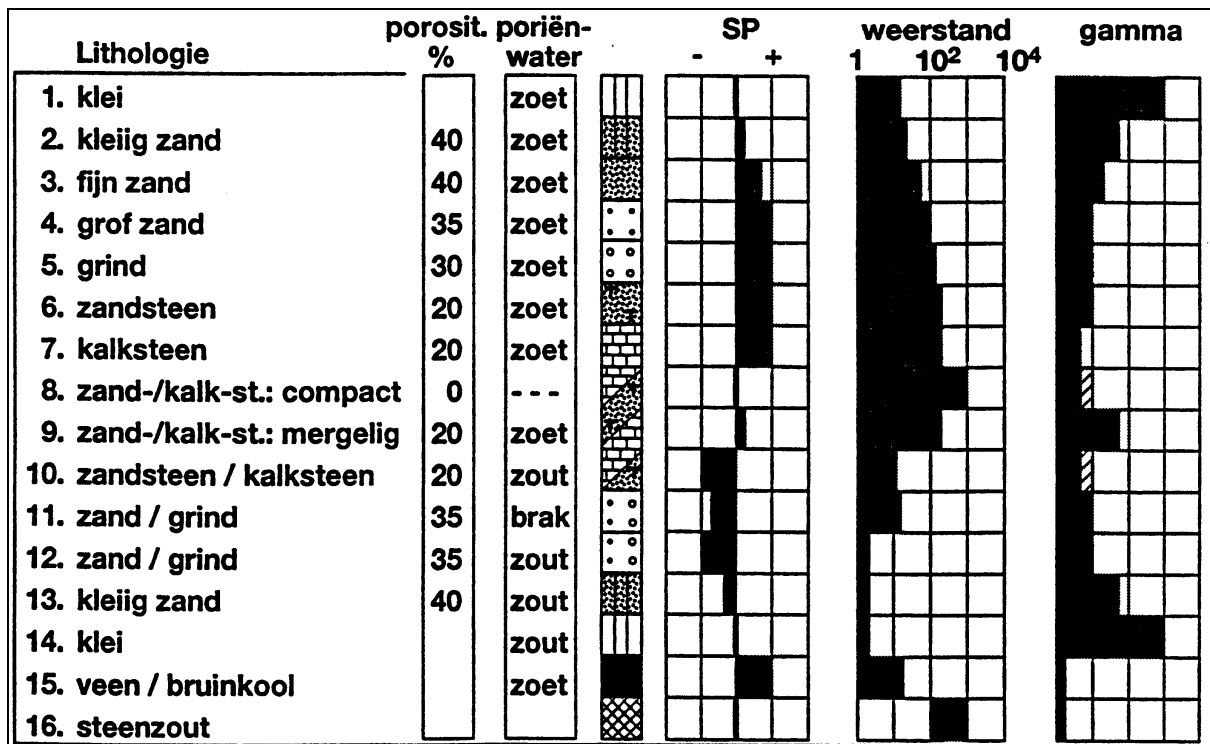
Lithologie	porosit. %	poriën-water	SP − +	weerstand 1 10² 10⁴	gamma
1. klei		zoet			
2. kleiig zand	40	zoet			
3. fijn zand	40	zoet			
4. grof zand	35	zoet			
5. grind	30	zoet			
6. zandsteen	20	zoet			
7. kalksteen	20	zoet			
8. zand-/kalk-st.: compact	0	- - -			
9. zand-/kalk-st.: mergelig	20	zoet			
10. zandsteen / kalksteen	20	zout			
11. zand / grind	35	brak			
12. zand / grind	35	zout			
13. kleiig zand	40	zout			
14. klei		zout			
15. veen / bruinkool		zoet			
16. steenzout					

Figure 9B. 13: Lithology recognition based on SP, Resistivity and GR.

In addition to aquifer delineation the gamma-ray log can also be used to determine the shaliness of the sand layers using the technique already described in the chapters 6 and 8.

9B.3.4.3 LITHOLOGY
The SN and LN resistivity logs are adversely affected by the borehole conductivity, however if the contrast between the borehole fluid conductivity and formation conductivity is not excessive, corrections can be applied, and a reliable estimate of the formation resistivity can be obtained. The resistivity in combination with the SP and GR is used to get an indication of the lithology. Fortunately the lithologies commonly encountered in the shallow subsurface of the Netherlands all have a rather unique signature. Based on the readings of the resistivity, SP and GR logs some 16 different lithologies can be recognised as shown in figure 9B.12. The major effects are:
- the increase in GR with shaliness,
- the decrease in resistivity with water salinity, and,
- a change in SP polarity from fresh to salt water bearing formations.

In hard rock it is often unavoidable to use a gamma-gamma density tool to determine the porous zones. However, in hard rock the risk of losing the tool and therefore the radioactive source is fortunately much smaller than in unconsolidated formations. Nevertheless the use of the radioactive sources in wells that penetrate potable water aquifers is only permitted after written approval of the designated authorities, like the NRC (Nuclear Regulatory Authority) in the USA.

9B.3.4.4 WATER SALINITY & HARDNESS
The SP log can in principle be used to derive the resistivity of the water in the pores of the formation. The advantage of this method, as explained in Chapter 5, is that no prior knowledge of other formation parameters such as porosity is required. The difference of the SP potentials E between a shale and a sand is related to the resistivity if the mudfiltrate R_{mf} and the resistivity of the water in the aquifer R_w.

$$E = (-71).log\frac{R_{mf}}{R_w}$$

(eq. 9B.11)

In this equation both R_w and R_{mf} are valid only for the same downhole temperature conditions. Empirical relations for the calculation of R_w are :

$$R_w = R_{mf} \, / \, 10^{(\,SP/-70.7\,)} \qquad \text{(eq. 9B.12)}$$

$$R_w^{NaCl} = 0.825 * (\,R_{we}^{1.227}\,) \qquad \text{(eq. 9B.13)}$$

$$R_w^{NaHCO_3} = 1.18 * R_w^{NaCl} \qquad \text{(eq. 9B.14)}$$

In which R_w^{NaCl} and $R_w^{NaHCO_3}$ are the equivalent formation water resistivity for NaCl and NaHCO$_3$ solutions respectively. They can be converted to salinities using standard charts. In oil-field operations the mud composition is well known and the mud usually contains enough solid particles to build up a mudcake. This mudcake prevents the continuous loss of borehole fluid and continuous dilution of the water in the pores. However, in water well operations the mud composition is often not precisely known. In addition, the mud normally does not contain enough solids to build up a stable mudcake. Hence if a salt water layer is encountered the fresh water filtrate from the mud will continue to dilute the salinity till hydrostatic equilibrium is reached. Despite these limitations a first estimate of water salinity should always be made if a reliable SP is available.

Dealing with only one pore fluid namely water occupying the pore space for 100 % has the advantage that the Archie/Humble equations, discussed in Chapter 5, are minimised to the first equation:

$$F = \frac{R_o}{R_w} = \frac{a}{\Phi^m} \qquad \text{(eq. 9B.15)}$$

In which :   dimension
m : the cementation factor   (d.l.)
R_o : the resistivity of a sand layer 100% filled with water   (ohm.m)
R_w : pore water resistivity   (ohm.m)
"a"   : the texture coefficient and   (d.l.)
Φ : the porosity   (d.l.)

For unconsolidated Rhine and dune sands, which are prominent in the Netherlands the following empirical relation was found :

$$F = \frac{1.26}{\Phi^{1.2}} \qquad \text{(eq. 9B.16)}$$

In hard rocks like hilly areas, away from the deltaic environments, the oil-field relations can be used :

$$F = \frac{0.62}{\Phi^{2.15}} \qquad \text{(eq. 9B.17)}$$

If the grain-size is known from cutting descriptions a reasonable approximation of the porosity can be made using the empirical relationship :

$$F = 33 - 15 \, LOG \, (D_{DOM}) \qquad \text{(eq. 9B.18)}$$

D_{dom} is the dominant grain-size in mm. Relation 9B.18 can be used to estimate the porosity. When this value is entered in the equations 9B.16 or 9B.17, the F factor is calculated. The value for F and the resistivity of the formation R_o measured in the well are both entered in equation 9B.16 to determine the resistivity of the water R_w. This R_w value can finally be converted to the water salinity using the relation depicted in figure 9B.19. One should realise that the accuracy of this method to calculate the water salinity should be considered as an indication, due to the many conversions and empirical relations that are used in this complicated calculation scheme. For low chlorine contents (< 50 ppm NaCl eq.) the inverse of the water resistivity R_w in Ohmm, is multiplied by 10^4 to obtain

conductivities "σ" expressed in µS/cm. The resulting value can then be used to obtain a direct estimate of the water hardness H°(D) by entering "s" in graph or figure 9B.11.

9B.3.4.5 POROSITY OF AQUIFERS

As mentioned in the introduction density and neutron porosity tools with chemical radioactive sources, the main sources of porosity information in oil fields, can often not be used in water wells for environmental reasons. Sonic tools do not suffer from this restriction, but in very

Lithology	F	grainsize from fig. 16.7 mm	Permeability k Darcy
gravel with sand	7.5	3.00	large
coarse sand with gravel	6	0.70	200
coarse sand	5	0.20	50
medium sand	4	0.05	25
fine sand	3.5	0.01	10

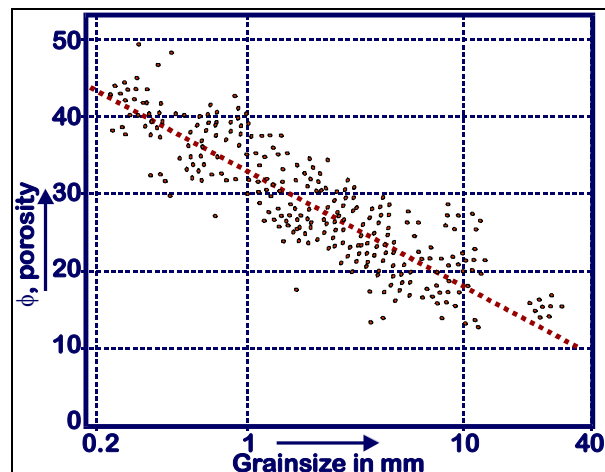Table 9B. 3: Comparison formation factors, grain-size, lithology, and permeability

unconsolidated sediments encountered in most water wells in The Netherlands, the Wyllie and Raymond Hunt equations that relate sonic travel time to porosity are not valid. Transmission of sonic

waves in very unconsolidated sediments is under these conditions dominated by compaction and not anymore by porosity. In hard rocks a simple slimline (2 1/8") tool with two receivers and one detector can be applied. The Wily equation (8.33) is then used for porosity calculations :

$$\varphi = \frac{\Delta T - \Delta T_{ma}}{\Delta T_{fl} - \Delta T_{ma}} \qquad \text{(eq. 9B.19)}$$

where:

ϕ : porosity, fraction of bulk volume (fr.b.v)

ΔT : transit time of the log [slowness in ms/ft]; slowness is defined as the reciprocal of the velocity (1/velocity)

ΔT_{ma} : transit time of the matrix

ΔT_{fl} : transit time of the fluid

Figure 9B. 14: Porosity as a function of grainsize

A reasonable estimate of porosity in clean sands can be obtained by using the dominant grain-size as explained in the previous section (eq. 9B.18). If the water salinity (R_w) is known the porosity could in principle be derived from the formation resistivity R_o using the equations 9B.11 to 9B.14.

R_o can be measured with the SN and LN resistivity logging tools. In that case the effect of the borehole is assumed to be negligible. In this method it is also expected that the coefficients "a" and "m" are already determined by laboratory analysis on undisturbed soil samples. The latter circumstances are not often fulfilled especially in exploratory ground water wells.
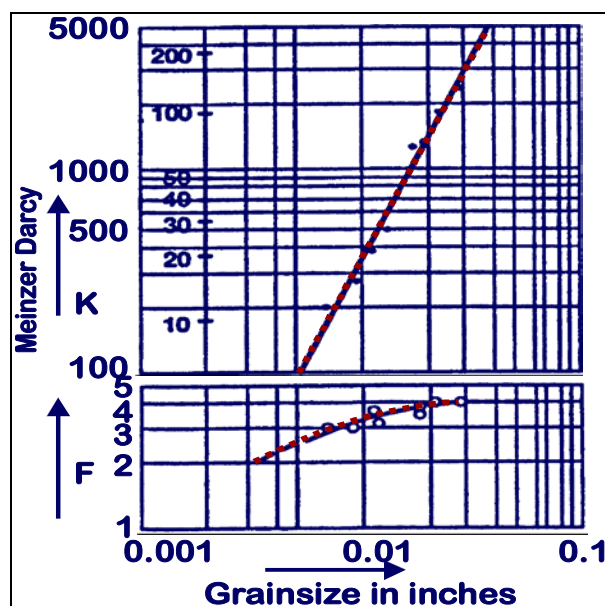

Figure 9B. 15: Permeability and formation factor versus grainsize

9B.3.4.6 PERMEABILITY AND & GRAIN-SIZE DISTRIBUTION

The formation factor F depends on both porosity and on the matrix texture. The latter parameter in turn depends on compaction, sorting and grain-size of the clastic sediments such as gravel, sand and silts. Again we are fortunate that prolific aquifers, which are the main target of our hydrological log evaluation, consist mainly of clean gravel and sand. Therefore the formation factor "*F*" can be related to the grain-size and permeability using empirical relationships. These relations proved to be valid in Dutch dune sands and Rhine sand deposits. Examples of the relations between "F" & "k" with grain-size are shown in the figures 9B.24 and 9B.25.
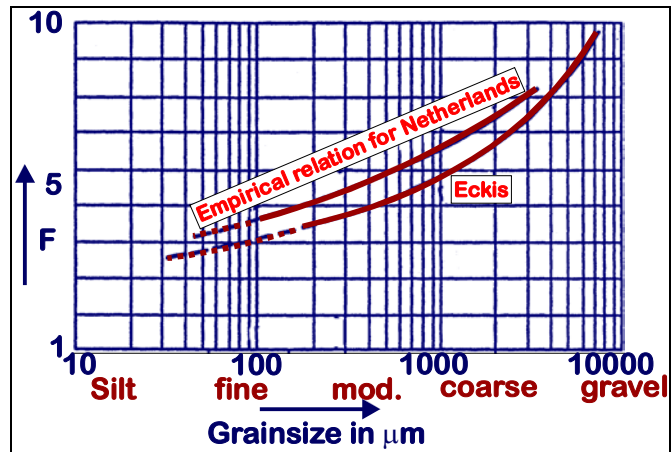
Figure 9B. 16: Formation factor versus grain size

9B.3.5 CASED HOLE LOG INTERPRETATION

9B.3.5.1 THE SPINNER

The most common tool used for flow measurements is the spinner tool, depicted in figure 9B.16. This tool consists of a tube in which a propeller (impeller) is mounted. The water that flows through the well and this tube will spin the propeller and the r.p.m. (revolutions per minute) of the spinner are recorded as a function of depth at the surface. By moving the spinner tool through the well differences in flow velocity can be observed. An example of a flow-log is shown in Figure 9B.17.

Oil field interpretations of the flow logs are often hampered by the presence of gas that has an unpredictable effect on the spinner. For water wells we deal with one fluid and the flow-log can be relatively easily calibrated if the total outflow of the well is measured on the surface. The cumulative production can then be smeared out over the productive intervals proportional to the ratio of r.p.m's over the various intervals and
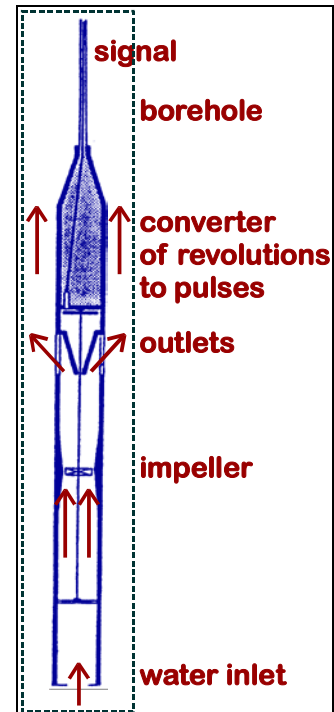

Figure 9B. 17:
Flow meter probe

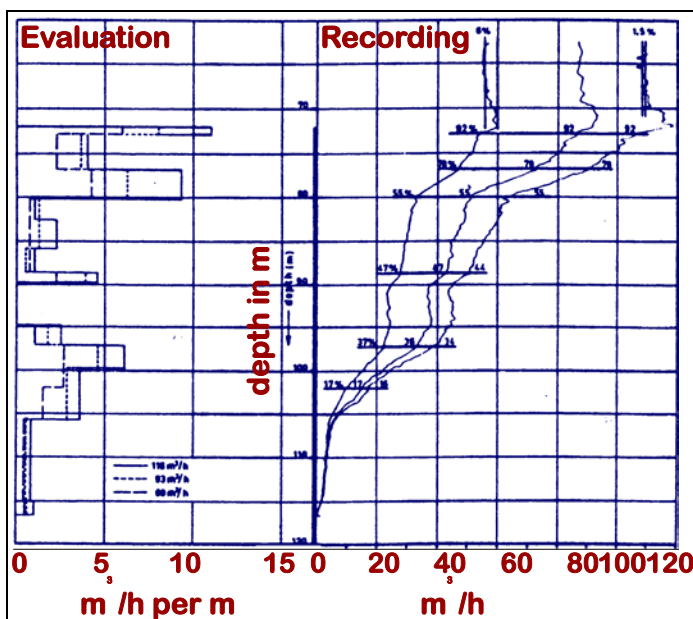the maximum r.p.m's measured above the shallowest productive interval.

Figure 9B. 18: Example of a flow log

9B.3.5.2 CONDUCTIVITY & THERMAL FLOW-METERS

Dealing with one fluid with a low salinity, as is ordinarily the case in water wells, has the advantage that brine slugs can be used as tracers. The use of radioactive tracers as is occasionally applied in oil wells would of course be impossible for environmental reasons. When the brine slug technique is executed a hose is run in the well connected to a tank filled with brine on the surface. Small quantities of brine are injected in the well and will move to the surface together with the fresh water from the various producing intervals. A fluid conductivity cell, often incorporated in the tube of the spinner flow meter, is used to detect the salinity spikes. The time required for the salinity spike to travel from one conductivity cell to the next is a good fluid-velocity indicator. The method is adversely affected by the dilution of brine opposite long producing intervals.

A third flow meter is based on measuring temperature differences and is therefore called the thermal flow meter. This tool is based on a differentiating method equivalent to the brine spiking method. The tube of the flow meter is in this case equipped with a heating element on the bottom and with temperature measuring devices higher up the tube. A small slug of heated water will travel along the tube and the difference in arrival times detected with two termistors will indicate the flow velocity in that part of the well.
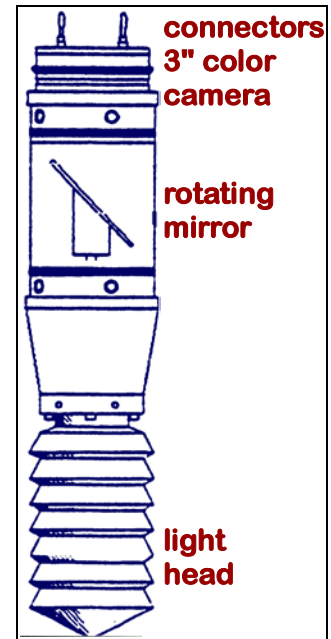

Figure 9B. 19: Schematic view of a borehole video camera.

9B.3.5.1 VIDEO & FLOW-VISION (VIDEO FLOW-METER) LOGS

In contrast with oil-well logging, water wells by nature contain a clear fluid in which video cameras will produce a discernible picture. The camera is placed along the tool axis and a series of pictures of the borehole wall is obtained with a rotating mirror. This set-up is shown in figure 9B.18. A Japanese firm introduced a tool with a fixed camera opposite a fixed conical mirror. This tool is much more rigid and can be run faster. The picture produced by this set-up is strongly deformed and can only be reviewed after digitising and electronic reformation. A video can be made while the tool is run into the well. The pictures are used for casing inspection, to check the condition of screens, which can be plugged by scale, and to see water inflow points. A non-polluting visible tracer can be inserted in the flow, and the movement of the tracer can tracked with successive video frames. The movement of the traces divided by the time interval between one or more frames gives the water velocity. This method is very valuable to determine very small aquifer movements, in which pollution has occurred.

9B.3.5.2 BOREHOLE TELEVIEWER

The name of this device is misleading due to the association with television. This tool gives no optical picture but an acoustic "impedance map" of the borehole wall or casing. The principle of the method is illustrated in figure 9B.19. The tool contains a transducer that sends out acoustic some 500 pulses per second in the 500 - 1000 kHz range. The pulses reflect from the borehole wall. Both, the total time it takes for the pulse to travel to the wall and back (transit time), and the amplitude of the reflected pulse, are recorded. To cover the entire borehole wall the transducer is directed to the wall and rotated over 360° some 3 to 5 times per second while the tool is constantly moving up the hole. The picture shown in figure 9B.19 is the reflection of the
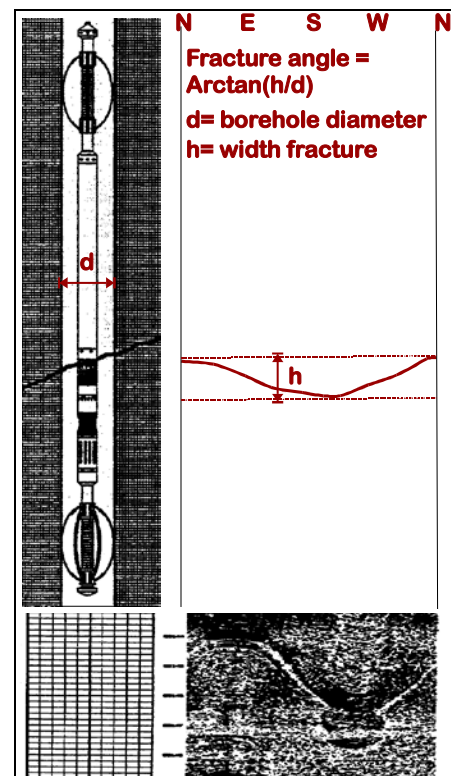

Figure 9B. 20: Typical BHTV log

borehole wall recorded as a cylinder, which is vertically sliced open and unrolled. An open fracture, intersecting the borehole in a plane, gives a low reflection sinusoidal signature as shown.

9B.3.5.3 PERMANENTLY INSTALLED ELECTRODE ARRAYS

- In the dunes along the sea, which are used for water filtering, saltwater can invade under the fresh water aquifer, when the fresh water is pumped away too fast.
- In the "polders" behind the dikes "kwel" or salt water can seep under the dikes if the dewatering via the canals removes too much fresh surface water.

In these sensitive areas it is important to monitor the position of the interface between fresh and salt water on a continuous basis. This is achieved by installing an array of electrodes permanently in observation wells. The electronic equipment on the surface measures the conductivity between the electrode pairs that are distributed over the survey interval as shown in figure 9B.20. In figure 9B.21 two resistivity profiles, which are measured 3 months apart, have been plotted. It is clear from this time lapse survey that the saltwater front marked by the low resistivities moved about 2 meters upward in the 3 months period.
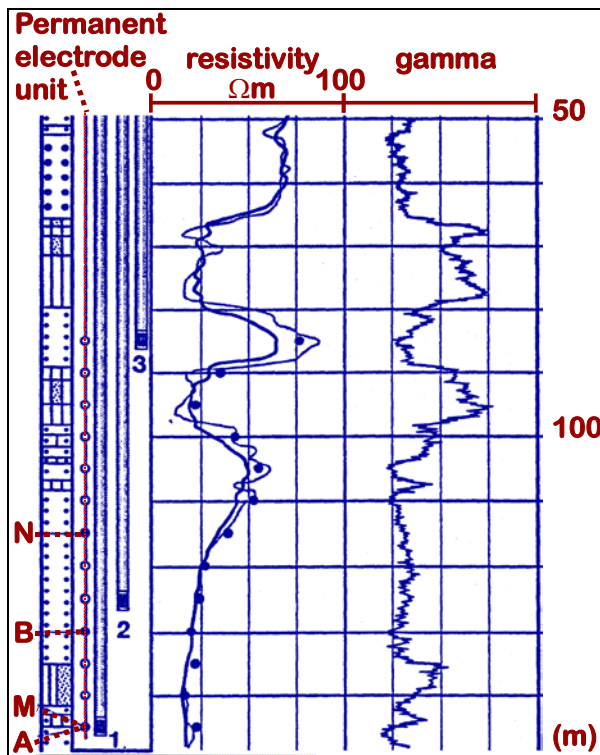

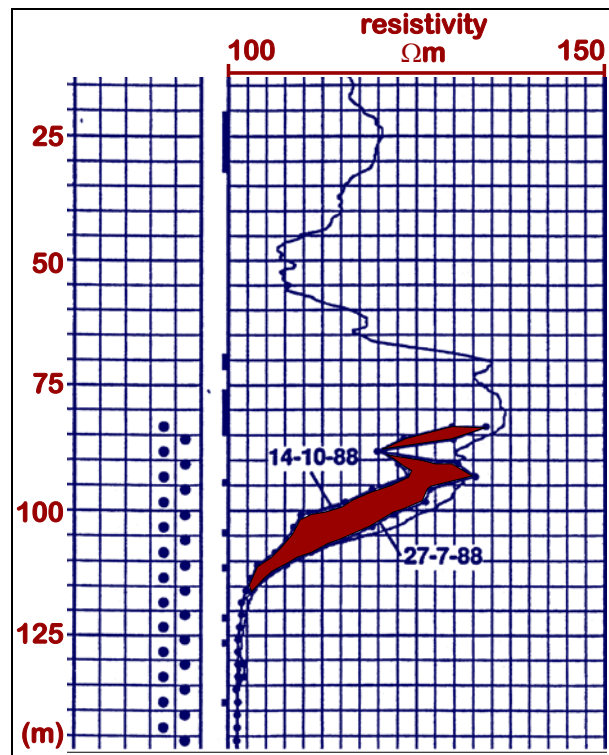Figure 9B. 21: Monitoring well for the detection of salt-water penetration in fresh water zones.

Figure 9B. 22: Time lapse survey of a salt-water detector